PART I

ELECTRONIC AND SPIN STATES

1

UV–VISIBLE ABSORPTION AND EMISSION ENERGIES IN CONDENSED PHASE BY PCM/TD-DFT METHODS

ROBERTO IMPROTA

CNR—Consiglio Nazionale della Ricerche, Istituto Biostrutture e Bioimmagini, Naples, Italy

1.1 Introduction
1.2 Quantum Mechanical Methods for Study of Electronic Excited States
1.3 Time-Dependent DFT
    1.3.1 Foundations of Time-Dependent DFT
    1.3.2 Limitations of Time-Dependent DFT
1.4 Solvation Models
    1.4.1 SS-PCM/TD-DFT
    1.4.2 LR-PCM/TD-DFT
1.5 Computing Spectra: Theory
    1.5.1 Choice of Functional
    1.5.2 Choice of Basis Set
    1.5.3 Choice of Solvation Model
1.6 Computing Spectra: Applications
    1.6.1 Selected Examples
        1.6.1.1 Bases of Nucleic Acids
        1.6.1.2 Coumarins
    1.6.2 Dealing with Supramolecular Interactions: Optical Properties of DNA
1.7 Concluding Remarks
References

Computational Strategies for Spectroscopy: From Small Molecules to Nano Systems, First Edition. Edited by Vincenzo Barone.

1.1 INTRODUCTION

The absorption and emission of light in the ultraviolet–visible (UV–vis) energy range (200–750 nm, 6.2–1.6 eV) are probably the 'most popular' spectroscopic processes which are continuously experienced by living beings in every-day life. For example, the existence of colors and the possibility of seeing depend on these processes.

From a scientific perspective, absorption and fluorescence spectra are a source of fundamental information in many chemical–physical molecular features [1–3]. First, they are two of the most straightforward methods of identifying a compound and thus represent key analytical techniques. Furthermore, advances in pump–probe time-resolved experiments have made absorption and fluorescence spectroscopy ideal tools to monitor the time evolution and outcome of many reactive processes [4]. These techniques can also provide indications of the electronic structure of molecules, their ground- and excited-state geometry, and the most relevant vibrational features, just to name a few basic properties.

From a complementary point of view, absorption spectra are often recorded to investigate the interactions between a molecule and its environment, and part of these interactions are indeed revealed by modifications of diagnostic molecular vibrations [5, 6]. Measuring absorption and fluorescence spectra is thus one of the first and key steps in many different areas of molecular and biological physics and nanotechnology science.

UV–vis absorption and emission are also extremely important from a technological and industrial point of view, as shown, for example, by the huge efforts made in the design of new dyes [7] or new photovoltaic materials [8], in the fields of light-emitting diodes [9] and phototropic materials, or, concerning pharmaceutical research, in the fields of photodynamic therapy [10] and molecular imaging [11].

The absorption and emission of light by molecules obviously depend on a basic quantum mechanical property, that is, the existence of discrete energy levels. It is not surprising that these processes have also been investigated from a theoretical/computational point of view. Computation of absorption and emission spectra is thus a very well developed research field, and an increasing number of theoretical and computational advances have made computational approaches a fundamental complement of experiments [12–32]. Schematically, we can say that computations have been shown to be able to:

1. Significantly help in the assignment of experimental spectra. Consider, for example, a complex organic reaction with multiple possible products (or a mixture of products), exhibiting different, though similar, absorption (or fluorescence) spectra. Comparison between the spectra computed for the most likely products and the experimental ones often provides fundamental information for identifying the products [33].
2. Increase the amount of information derived from experiments. Due to the large number and complexity of the effects that can potentially influence absorption and emission spectra, it is not always easy to disclose all the information thereby contained, limiting the potentialities of these techniques. This is true

especially in the condensed phase, where many fundamental features are often somewhat hidden in broad and structureless spectra. In such a scenario, being able to accurately compute spectra (possibly vibrationally resolved) is extremely useful.

3. Shed light on the relationship between the structure of a compound and its spectral properties. Computations can more easily dissect the different chemical–physical effects (intrinsic and environmental) modulating the spectral properties of molecule. They can thus help the design of new compounds with specifically tailored features (e.g., new dyes), with significant benefits for industrial research.

On the other hand, notwithstanding the huge theoretical and computational efforts, a reliable calculation of absorption and emission spectra, especially when dealing with sizable molecules, is not a trivial task. In fact, while it is relatively easy to approach the so-called chemical accuracy for molecules in the ground electronic states, an accurate determination of the energy of the excited electronic states is computationally and theoretically much more demanding. Indeed, excited electronic states are often quite close in energy: The energy ordering often depends on fine details of the adopted computational method (e.g., the size of the basis set). The breaking of the Born–Oppenheimer approximation is rather common, and nonadiabatic couplings cannot be safely neglected [13]. Furthermore, not only for computing emission spectra but also for obtaining the Franck–Condon factors between the ground and the electronic excited states, the excited-state stationary points are needed, and, thus, performing excited-state geometry optimizations is often necessary. In this respect, analytical excited-state gradients are available only for a limited number of methods (CIS, CASSCF, CASPT2, SAC-CI, CC2) [29–40].[1] Finally, the most accurate ab initio methods are too computationally expensive for studying the excited states of most systems of technological and biological processes, which are usually medium/large-size molecules.

The usefulness of computational methods would of course be quite limited if environmental effects could not be taken into proper account, since almost all of the above-mentioned processes occur in solution. As a consequence, even a qualitative agreement with experiments requires the use of a suitable solvation model. The inclusion of environmental effects involves additional difficulties: Not only should the solvation model be able to provide an accuracy comparable to that attained in vacuo, but in solution any problem involving excited states becomes intrinsically dynamic [41]. The solvent reaction field couples the ground-state density with the density correction and the orbital relaxation arising from the electronic transition. Furthermore, the coupling is modulated by the solvent relaxation times [41].

However, thanks to very recent methodological and computational advances [especially in the methods rooted in the time-dependent density functional theory

[1] Configuration interaction singles (CISs); complete active-space self-consistent field (CASSCF) and its second-order perturbation counterpart (CASPT2); symmetry-adapted cluster configuration interaction (SAC-CI); double coupled cluster (CC2).

(TD-DFT)][17, 18] it is nowadays possible to compute remarkably accurate absorption and emission spectra of sizable molecules in solution. Furthermore, the inclusion of these methods in user-friendly computational methods has made these techniques available to nonspecialists.

In this chapter we shall thus discuss some suitable strategies for computing the absorption and emission spectra of medium–large systems in "complex" environment, focusing on the computation of the vertical excitation energies and the vertical emission energies. Treatment of the lineshape can be found in the Chapters 8 and 10.

1.2 QUANTUM MECHANICAL METHODS FOR STUDY OF ELECTRONIC EXCITED STATES

A real "panoplia" of quantum mechanical methods for computing the properties (energy, oscillator strengths, eventually the minima, etc.) of the excited electronic states of medium-size molecules is currently available. A detailed discussion of the main features of each computational approach is obviously outside the scope of this chapter, and many interesting books and review articles are already available within the literature [12–32, 42, 43]. Very schematically, we can distinguish between wavefunction-based methods and electron-density-based methods. In some methods of the former family, such as single-reference configuration interaction (CI) or multiconfigurational-based ones—multiconfigurational SCF (MCSCF), for example, the CASSCF, CASPT2 [14–16], or multireference CI [19]—any electronic state is described as the combination of several Slater determinants corresponding to different electronic configurations (i.e., different occupation schemes of the molecular orbitals, MOs). The expansion coefficients of the different Slater determinants and, in multiconfigurational SCF approaches, the expansion coefficients of the MOs in the Slater determinants are then variationally computed.

A different approach is followed by other wavefunction-based methods as those belonging to the coupled-cluster (CC) family [20, 21, 28]. CC models are based on the single-reference wavefunction and allow us to compute excitation energies within the equation-of-motion [24–26] and linear response [27] CC formalisms (EOM-CC and LR-CC, respectively). Accuracy of CC results depends on the level of truncation in the CC expansion. In this respect, extensions of CC theory for excited states to include triplet excitations within both iterative and noninterative schemes [26, 27] allow for very accurate computations of excited-state properties. However, due to their high computational cost, these methods cannot be applied to large molecules. Recently, promising results have been obtained by an approximated single and double CC method, which, exploiting the resolution of the identity (RI) approximation for two electron integrals, can be applied to fairly large systems with a good degree of accuracy [22, 23]. Additionally, the SAC-CI approach [34], being formally equivalent to EOM-CC and LR-CC models, introduces some approximations by neglecting the unimportant unlinked terms and the perturbation selection of the linked operators. By doing so, the computations become more efficient and allow studies of larger and

more complex systems, which are further facilitated by the availability of SAC-CI analytical gradients [35].

The simpler wavefunction method is CIS, where the excited states are computed by considering only single excited Slater determinants using the HF MO to describe the ground state. Despite exhibiting some advantages (limited computational cost, size consistency, availability of analytical first and second derivatives), CIS excitation energies are not very accurate, being usually overestimated by 0.5–2 eV (see Dreuw and Head-Gordon [29] for a more detailed discussion).

A second class of methods is instead based on the knowledge of the electron density in a theoretical framework similar to that of the DFT. In DFT the effects of the exchange and of the electronic correlation are included by the so-called exchange-correlation (xc) functional, which is obtained by an empirical fit of experimental data or by imposing some physical constrains based on the behavior of some "limit" model systems [44]. For the excited states, the TD-DFT [17, 18] recently emerged as a very effective tool, since, when coupled to suitable density functionals, it often reaches an accuracy comparable to that of the most sophisticated (but expensive) post-Hartree–Fock methods [45–59], with a much more limited computational cost. As a consequence in the last years an increasing number of TD-DFT applications have appeared in the literature, also because this method can be used as a "blackbox" and is thus also easily accessible to nonspecialists.

TD-DFT has often been criticized for not being a first-principle nonempirical method (in analogy with its "parent" DFT), not showing uniform accuracy in treating electronic transitions with different characters, and delivering a qualitatively wrong description of the crossing region between different electronic excited states (see below). On the other hand, although wavefunction-based methods have known impressive methodological advances, significantly increasing their range of applicability, they suffer from very high computational costs. As a consequence, some compromises concerning the basis set or, for MC methods, the active space employed are often necessary, not only decreasing the expected accuracy but also introducing a significant degree of arbitrariness in formally rigorous methods. Furthermore, semiempirical parameters are often also present in sophisticated calculations, such as CASPT2, which often include the so-called IPEA shift. This empirical parameter has been introduced to compensate for systematic errors in CASPT2 ionization potentials (IPs) and electron affinities (EAs). Its application typically increases the computed CASPT2 excitation energies by about 0.1–0.3 eV and corrects for the known tendency of CASPT2 to slightly underestimate excitation energies.

In our opinion, each method has its own advantages and limitations, and the choice of quantum mechanical (QM) method depends on the phenomena/system investigated. As discussed in the introduction, a method coupling accuracy and computational feasibility is necessary when treating systems of biological and technological interest. On the grounds of our experience, we think that TD-DFT probably represents the best compromise between accuracy and computational cost for describing the excited-state behavior in medium/large-size molecules. As a consequence it will be used as reference computational method in this chapter.

1.3 TIME-DEPENDENT DFT

1.3.1 Foundations of Time-Dependent DFT

TD-DFT has been reviewed in several excellent papers [17, 18]. We thus limit ourselves to its basic foundations.

TD-DFT is rooted in the Runge–Gross theorem [60] (which is not valid for the degenerate ground state), allowing the extension of the Hohemberg–Kohn–Sham formulation of the TD-DFT theory to the treatment of time-dependent phenomena:

$$\Psi(t) = e^{-i\phi(t)}\Psi[\rho, \Psi_0](t) \tag{1.1}$$

The Runge–Gross theorem implies that:

(a) A functional of the time dependent charge density, ρ, determines the wave-function up to a time-dependent phase factor.
(b) All the observables can be calculated with knowledge of the time-dependent one-body density.

When dealing with time-independent processes, we can determine the ground state of a given system by minimizing its total energy. In time-dependent systems no variational principle based on the energy can be exploited, since the total energy is not a conserved quantity. It is possible, however, to resort to another quantity, that is, the quantum mechanical action:

$$[\Psi] = \int_{t_0}^{t_1} dt \langle \Psi(t)| \frac{\partial}{\partial t} - \hat{\mathcal{H}}(t)|\Psi(t)\rangle \tag{1.2}$$

The true time-dependent density is that making the action stationary:

$$\frac{\delta A}{\delta \rho(\mathbf{r}, t)} = 0 \tag{1.3}$$

On the grounds of the Runge–Grosse theorem, it is then quite straightforward to derive the time-dependent Kohn–Sham equation, in analogy with the procedure used in TD-DFT. For adiabatically introduced perturbations, whose frequency does not exceed the highest occupied–lowest occupied molecular orbital (HOMO–LUMO) gap, it is possible thus to assume the existence of a potential v_{eff} ($\mathbf{r}$, t) for an independent particle system whose orbitals ψ_i ($\mathbf{r}$, t) yield the same charge density ρ ($\mathbf{r}$, t) as for the interacting system,

$$\rho(\mathbf{r}, t) = \sum_i f_i |\psi_i(\mathbf{r}, t|^2 \tag{1.4}$$

Minimizing the action, we then obtain

$$\left[-\frac{1}{2}\nabla^2 + v_{\text{eff}}(\mathbf{r}, t) \right] \psi_i(\mathbf{r}, t) = i \frac{\partial \psi_i(\mathbf{r}, t)}{\partial t} \tag{1.5}$$

The first term on the left-hand side of Eq. 1.5 represents the kinetic energy of the electrons, whereas the second one, v_{eff}, is given as

$$v_{\text{eff}} = v_{\text{ext}}(\mathbf{r}, t) + \int \frac{\rho(\mathbf{r}, t)}{|r - r'|} dr' + v_{\text{xc}}(\mathbf{r}, t) \tag{1.6}$$

where v_{ext} is the external potential (electron–nuclei interaction), the second term gives account of the electron–electron Coulomb interaction, and the third one, v_{xc}, represents the time-dependent counterpart of the stationary exchange–correlation functionals

$$v_{\text{xc}}(\mathbf{r}, t) = \frac{\delta A_{\text{xc}}[\rho]}{\delta \rho(\mathbf{r}, t)} \tag{1.7}$$

$$A_{\text{xc}} = \int_{t_0}^{t_1} E_{\text{xc}}[\rho_t] dt \tag{1.8}$$

Up to this point, no approximation has been made in TD-DFT: As in DFT, the only problem is the knowledge of the xc functional. However, in the most commonly used approaches, the determination of the time-dependent xc functional involves additional approximations. The simplest approximation is the adiabatic approximation, which can be applied if the external potential varies slowly in time [61]. It is a local approximation in time, assuming that v_{xc} is determined only by the density $\rho(t)$ at the same time,

$$v_{\text{xc}}[\rho](\mathbf{r}, t) = \frac{\partial A_{\text{xc}}[\rho]}{\partial \rho(\mathbf{r}, t)} \simeq = \frac{\partial E_{\text{xc}}[\rho]}{\partial \rho_t(\mathbf{r})} = v_{\text{xc}}[\rho_t](\mathbf{r}) \tag{1.9}$$

From the physical point view, the adiabatic approximation assumes that the reaction of the SCF to temporal changes in ρ is instantaneous, neglecting all the retardation effects.

Most of the TD-DFT implementations compute the excitation energies relying on a second approximation, based on the linear response theory.

For a small external time-dependent potential it is not necessary to solve the full time-dependent KS equation, but most time-dependent properties can be calculated from the first-order variation of the density:

$$\delta P_{ij}(\omega) = \frac{n_j - n_i}{\omega - (\epsilon_i - \epsilon_j)} [\delta \mu_{\text{ext}}(\omega) + \delta v_{\text{scf}}(\omega)] \tag{1.10}$$

where δP_{ij} is the linear response of the density matrix in the frequency domain and δv_{scf} is the linear response of the SCF due to the change in the charge density.

On the other hand, δv_{scf} depends on the response of the density matrix,

$$\delta v_{\text{scf}}^{ij} = \sum_{k,l} K_{ij,kl}(\omega)\, \delta P_{kl} \tag{1.11}$$

The above equations are usually expressed in matrix from:

$$\begin{bmatrix} \mathbf{A} & \mathbf{B} \\ \mathbf{B} & \mathbf{A} \end{bmatrix} \begin{bmatrix} \mathbf{X} \\ \mathbf{Y} \end{bmatrix} = \omega \begin{bmatrix} 1 & 0 \\ 0 & -1 \end{bmatrix} \begin{bmatrix} \mathbf{X} \\ \mathbf{Y} \end{bmatrix} \tag{1.12}$$

where vectors **X** and **Y** represent the linear response of the density matrix to the time-dependent perturbation,

$$A_{ai,bj} = \delta_{ab}\delta_{ij}(\epsilon_a - \epsilon_i) + K_{ai,bj} \tag{1.13}$$

and

$$B_{ai,bj} = K_{ai,jb} \tag{1.14}$$

where ϵ is the energy of the time-independent KS orbitals (ψ), i, j referring to the occupied and a, b to the virtual orbitals.

Excitation energies are thus computed as poles of the dynamic polarizability, that is, as the values of ω leading to zero eigenvalues on the left-hand side of the matrix of Eq. 1.12. In the framework of the above equations, an efficient "fast" iterative solution for the lowest eigenvalue/excitation energies can be attained [62]. Oscillator strengths can also be obtained by the eigenvectors of Eq. 1.12, as explained by Casida [17].

The recent implementation of TD-DFT analytical gradients [38–40] allows for the determination of the excited-state stationary points and their properties (e.g., the multipole moments). Harmonic frequencies can be obtained by performing numerical differentiation of the analytic gradients, enabling us to perform the same kind of vibrational analysis performed in the ground electronic state [45–50].

TD-DFT calculations thus allow determining the energy and the properties of the excited states with a limited computational cost. As a consequence, it is usually not necessary to impose any symmetry constraint, very large basis sets can be used, and no ad hoc choice (see, e.g., the active space in CASSCF/CASPT2 calculations) is usually necessary, also when dealing with large-size systems. These are important features: On the one hand, it is possible to treat different systems (e.g., a supramolecular system and its component) and different kinds of transitions (e.g., $n\pi^*$ and $\pi\pi^*$) with a similar degree of accuracy, putting the analysis of the computational results on firmer ground. On the other hand, they make TD-DFT a very user-friendly method easily accessible to nonspecialists. As a consequence in the last years the number of TD-DFT studies has continuously increased, allowing important advances in our knowledge of the potentialities and the limitations of this method. It is nowadays well assessed that TD-DFT, when employing a suitable density functional, can provide fairly accurate results (with 0.2–0.3 eV the experimental results) in several classes of systems, despite the limited computational cost [51–58].

It is important, however, to remember that TD-DFT cannot be considered a blackbox method, since the accuracy of its results depends on several factors (functional, basis set, etc.) which have to be properly addressed. Furthermore, as

discussed in the next section, there are several systems/processes for which TD-DFT has often shown significant failures.

1.3.2 Limitations of Time-Dependent DFT

TD-DFT is a mono-determinantal method, and thus it cannot be applied to electronic states with an intrinsic multireference character [2]. Analogously, TD-DFT can exhibit deficiencies in treating electronic transitions with substantial contributions from double excitations [63–66], although interesting attempts to overcome the above limitations have been proposed [65–71]. In several cases, however, an electronic transition exhibits a multireference character (or a significant contribution from double excitations) just because of a poor description of the ground-state MO by HF orbitals, and such features are not present when using MOs computed at the DFT level.

Another traditional failure of TD-DFT concerns the treatment of long-range charge transfer (CT) transitions between zero-overlap donor–acceptor pair. Standard functionals significantly underestimate the transition energy and fail to reproduce the correct $1/R$ trend when the donor/acceptor distance (R) increases [29].

However, in the last five years new functionals have been developed, which are able to deliver a correct estimate also of the long-range CT transitions [72–76]. Furthermore, it is worth noting that for electronic transitions which involve only partial CT character, the underestimate of the excitation energies by TD-DFT may be controlled by the use of hybrid functionals, whereas the performances of pure functionals are much poorer (see next sections). Therefore, some of the deficiencies ascribed to TD-DFT are not intrinsic features of the method but depend on the choice of the functional.

Also "long-range" corrected functionals are not able, however, to accurately treat other classes of compounds such as cyanines, especially when the length of the ethylenic bridge connecting the two $NH_2{}^+/NH_2$ moieties increases. This failure is likely due to the intrinsic multideterminantal character of the electronic transitions in such molecules [58, 77].

1.4 SOLVATION MODELS

As anticipated in the introduction, since most of the UV–vis spectra are recorded in the condensed phase, suitable theoretical models, able to include the effect of the solvent on the absorption and the emission spectra, are necessary. This topic has been discussed in detail in several reviews, and thus, also in this case, we limit our discussion to some basic aspects [41, 78]. The most direct procedure to compute the spectra of a given molecule (the solute) in solution consists in including in the calculations a certain number of explicit solvent molecules [79, 80]. However, this approach has to face two severe difficulties: (i) the number of solvent molecules necessary to reproduce the bulk properties of a liquid (say, its macroscopic dielectric constant) is very large; (ii) a dynamical treatment averaging all the possible configurations of the solvent molecules is in principle necessary. As a consequence, this approach has a large computational cost, especially when used for studying

excited states, which, as discussed above, need rather expensive QM computational methods. As a consequence, this "purely supramolecular" approach usually relies on an approximate description of the solvent molecules by using classical force fields within a mixed quantum mechanics/molecular mechanics (QM/MM) mixed approach. However, correct placement of the first solvation shell molecule is required, which can often be a difficult task for the standard molecular mechanics force field [81]. Furthermore, a large number of QM/MM calculations are necessary to reach converged excitation energies.

Complementing the results obtained for the study of ground electronic states in solution, many computational studies indicate that approaches exploiting continuum solvation models are very effective tools for evaluating the solvent effect on the excited-state properties. Among continuum models, the polarizable continuum model (PCM) is probably the one most commonly used. In the following, we thus focus mainly on this method [78, 82].

In the PCM the solvent is described as a homogeneous dielectric which is polarized by the solute. The latter is placed within a cavity in the solvent medium (built as the envelope of spheres centered on the solute atoms) and the proper electrostatic problem at the cavity surface is solved using a boundary element approach [78]. In the PCM framework, the solvent loses its molecularity and, especially in hydrogen-bonding solvents, the explicit inclusion of solute–solvent interactions is very important for getting accurate results. In these cases, as discussed in detail in the next section, mixed discrete/continuum models, where a limited number of solvent molecules are included in the computational model, usually provide accurate results.

Inclusion of the solvent effect within a continuum model in time-dependent processes as absorption or emission poses several problems. On the one hand, the solution of the electrostatic problem is highly nonlinear. Indeed, the solvent reaction field should be variationally determined together with all the other parameters in the electronic method used (MO coefficients, CI coefficients, excitation amplitudes, etc), but all those parameters do depend on the solvent reaction field. Different approaches have been envisaged to tackle the above problem. The most used can be classified in two classes, that is, state-specific (SS) and linear response (LR) approaches [83–86]. In SS methods (e.g., CASSCF/PCM) a different effective Shrödinger equation is solved for each state of interest, achieving a fully variational formulation of solvent effect on the excited-state properties. In the methods exploiting the LR response formalism (as TD-DFT) the excitation energies are "directly" determined without computing the exact excited electron density. As discussed in more detail in the next sections, SS and LR methods can provide very different estimates of the solvent effect on the excited-state properties and dynamical solvation effects. This point should thus be treated very carefully when using PCM in excited-state calculations.

Dynamical Solvent Effect Another critical topic to be considered when studying excited states in solution is the dynamical solvent effect. Electron excitation is an intrinsically dynamic process: The full equilibration of solvent degrees of freedom to the excited-state density requires a finite time. It is thus fundamental that the characteristic times of solvent degrees of freedom are properly taken into account.

Several theoretical approaches to the description of dynamical solvent effects have been proposed within the framework of PCM of other continuum models [41]. The simplest, and most commonly used, treatment involves the definition of two limit time regimes: equilibrium (EQ) and nonequilibrium (NEQ). In the former all the solvent degrees of freedom are in equilibrium with the electron density of the excited-state density, and the solvent reaction field depends on the static dielectric constant of the embedding medium. In the latter, only solvent electronic polarization (fast degrees of freedom) is in equilibrium with the excited-state electron density of the solute, while the slow solvent degrees of freedom remain equilibrated with the ground-state electron density. In the NEQ time regime the "fast" solvent reaction field is ruled by the dielectric constant at optical frequency (ϵ_{opt}, usually related to the square of the solvent refractive index).

The NEQ limit is the most suitable to the treatment of the absorption process. The study of the fluorescence process is instead more complex, since in this case dynamical solvent effects cannot be rigorously decoupled from the intramolecular effects due to the motion of the wave-packet (WP) on the excited-state surface. However, it is possible to define some limit reference models, and intuitive consideration of the properties of the solvent and/or the excited potential energy surface is often sufficient to define what is the most suitable to the treat the case under study (see next sections). PCM can be used in conjunction with all the most important excited-state electronic methods. Since we selected TD-DFT as our reference electronic method, we shall treat PCM/TD-DFT in more detail in the next sections.

1.4.1 SS-PCM/TD-DFT

The solvent reaction field contribution to the solute free energy (G) can be expressed in PCM as

$$G = \tfrac{1}{2}\mathbf{V}^{\dagger}\mathbf{q} \tag{1.15}$$

where vector $\mathbf{V}$ collects the values of the solute's electrostatic potential and $\mathbf{q}$ is the apparent surface charge placed at the center of the surface *tesserae* (i.e., the small tiles which the cavity surface is finely subdivided in), where also $\mathbf{V}$ is computed.

In the latest version of the method [78] the polarization charges depend on the solute's electrostatic potential and, thus, on its density through a general relationship of the form

$$\mathbf{q} = -\mathbf{D}\mathbf{V} \tag{1.16}$$

where the square matrix $\mathbf{D}$ is related to cavity geometric parameters and the solvent dielectric constant ϵ.

Consider a generic excited electronic state (2) together with the corresponding ground state (1). As discussed by Improta et al. [86], in SS methods the excited-state equilibrium [$\mathcal{G}_{\text{eq}}(2)$] free energy in solution thus explicitly depends on the excited

state (2) density:

$$\mathcal{G}_{\text{eq}}^{(2)} = \frac{1}{2}\sum_i q_i^{(2)} V_{i,\rho}^{(2)} = \frac{1}{2}\sum_i q_{i,f}^{(2)} V_{i,\rho}^{(2)} + \frac{1}{2}\sum_i q_{i,s}^{(2)} V_{i,\rho}^{(2)} \tag{1.17}$$

The nonequilibrium ($\mathcal{G}_{\text{neq}}^{(2)}$) free energy in solution involves an explicit dependence on the density of the ground state (1):

$$\mathcal{G}_{\text{neq}}^{(2)} = \frac{1}{2}\sum_i q_{i,f}^{(2)} V_{i,\rho}^{(2)} + \left(\sum_i q_{i,s}^{(1)}\, V_{i,\rho}^{(2)} - \frac{1}{2}\sum_i q_{i,s}^{(1)} V_{i,\rho}^{(1)}\right) + \left(\frac{1}{2}\sum_i q_{i,s}^{(1)}\, V_{i,f}^{(2)} - \frac{1}{2}\sum_i q_{i,s}^{(1)}\, V_{i,f}^{(1)}\right) \tag{1.18}$$

In the above equations q_f/q_s and V_f/V_s are the polarization charges and the corresponding potentials relative to the "fast" and "slow" solvent degrees of freedom. The potential generated by the density of state (n) is given as $V_\rho^{(n)}$.

The absorption process is ruled by nonequilibrium solvation, and thus the solvent contribution to the vertical excitation energy can be computed by using the following relationship:

$$\Delta G_{\text{abs}} = \mathcal{G}_{\text{neq}}^{(2)} - \mathcal{G}_{\text{eq}}^{(1)} \tag{1.19}$$

Soon after the electronic transition has occurred, the system starts evolving on the excited-state potential energy surface (PES) toward its energy minimum. At the same time, slow solvent degrees of freedom start equilibrating on the excited-state electron density. These two processes cannot be rigorously decoupled, especially when they exhibit similar time scales, and we cannot thus expect that a single strategy is suitable to all the possible emission processes. In many cases, however, this complex scenario can be simplified by means of qualitative considerations on the properties of the solvent and/or the excited potential energy surface. The equilibration of intramolecular degrees of freedom is faster than solvent equilibration except for very flat PESs or when many low-frequency motions are involved (large-amplitude torsional motions, inversions, etc.). This is especially true in polar solvents and for electronic transitions involving significant variations of the excited-state electron density. In such cases, indeed, time-resolved experiments suggest that the equilibration of the slow solvent degrees of freedom occurs on the picosecond time scale. This time should be long enough to assume that the excited electronic state has reached its minimum. A simple limiting case is that of ultrafast excited-state decay when only fast solvent degrees of freedom are expected to be in equilibrium with the excited-state density. In this limit, ΔG_{em} can be computed exactly in the same way as ΔG_{abs} [86]:

$$\Delta G_{\text{em}} = \mathcal{G}_{\text{neq}}^{(2)} - \mathcal{G}_{\text{eq}}^{(1)} \tag{1.20}$$

Of course, in this case excited-state geometry optimizations should also be performed in the nonequilibrium limit.

Another simple limit is that of "very long" excited-state lifetimes, which characterize, for instance, strongly fluorescent species. In this case, we can assume that all the solvent degrees of freedom are in equilibrium with the excited-state density. The ground-state ($\mathcal{G}^{(1)}_{\text{neq}}$) nonequilibrium free energy in solution describing the emission process can thus be obtained from Eq. 1.18, interchanging labels 1 and 2. The fast solvent degrees of freedom are equilibrated with the ground-state electron density, whereas the slow ones are kept frozen at the value obtained in the equilibrium calculation of the excited state.

In this limit, excited-state geometry optimizations should be performed with the solvent equilibrium limit, and the solvent contribution to the fluorescence energy (ΔG_{em}) is given as

$$\Delta G_{\text{em}} = \mathcal{G}^{(2)}_{\text{eq}} - \mathcal{G}^{(1)}_{\text{neq}} \tag{1.21}$$

The above relationship is the most suitable for treating phosphorescence, where states (2) and (1) correspond to T_1 and S_0, respectively.

The computation of the quantities involved in Eqs. 1.20 and 1.21 is straightforward using a generalization of the SS-PCM/TD-DFT method presented elsewhere [86], where the nonlinear problem of determining the polarization charges corresponding to the excited-state density is solved by using a self-consistent iterative procedure. Starting from a TD-DFT calculation, a first approximation to the state-specific reaction field is computed using the electron density of the state of interest by solving Eq. 1.16. In the next step, a TD-DFT calculation is performed in the presence of this first set of polarization charges, providing an updated excited-state density and, consequently, a new set of polarization charges. This iterative procedure is continued until convergence on the reaction field is achieved. In the cases examined until now, 4/5 iterations are usually sufficient to reach a convergence ≤ 0.0001 a.u. on the final energy.

The final equilibrium and nonequilibrium energies of the state of interest are easily determined by adding the corrections obtained by Eq. 1.17 or 1.18 to the excited-state energy provided by the TD calculation.

1.4.2 LR-PCM/TD-DFT

In LR-PCM/TD-DFT the excitation energies are "directly" determined without computing the excited-state density by plugging in a PCM contribution in the TD-DFT equations reported in Section 3.1 [87]. The coupling matrix **K** of Eq. 1.11 can thus be decomposed in two terms, the former being related to the gas-phase calculation, the second related to PCM:

$$K_{st,uv} = K^0_{ai,bj} + K^{\text{PCM}}_{ai,bj} \tag{1.22}$$

The PCM contributions to the time-dependent Kohn–Sham equations depend [87] on the term $\delta\phi(\mathbf{s}', \omega)$,

$$\delta\phi(\mathbf{s}', \omega) = \int_{\mathbf{R}^3} \frac{\delta\rho^{\mathrm{el}}(\mathbf{r}', \omega)}{|\mathbf{s}' - \mathbf{r}'|} d\mathbf{r}' \tag{1.23}$$

which formally corresponds to an electrostatic potential computed using the electron density variation ($\delta\rho^{\mathrm{el}}$) associated with the electronic transition in place of a specific electron density (ρ^{el}). The contribution from the PCM operator is then defined as

$$v^{\mathrm{PCM}}\left[\delta\rho^{\mathrm{el}}\right](\mathbf{r}) = \int_\Gamma \int_\Gamma \delta\phi(\mathbf{s}', \omega)\mathcal{Q}(\epsilon_{\mathrm{opt}}; \mathbf{s}', \mathbf{s}) \frac{1}{|\mathbf{s} - \mathbf{r}|} d\mathbf{s}\, d\mathbf{s}' \tag{1.24}$$

if only the fast solvation degrees of freedom are equilibrated with the excited-state density of the solute, and

$$v^{\mathrm{PCM}}\left[\delta\rho^{\mathrm{el}}\right](\mathbf{r}) = \int_\Gamma \int_\Gamma \delta\phi(\mathbf{s}', \omega)\mathcal{Q}(\epsilon; \mathbf{s}', \mathbf{s}) \frac{1}{|\mathbf{s} - \mathbf{r}|} d\mathbf{s}\, d\mathbf{s}' \tag{1.25}$$

when treating equilibrium solvation. In the nonequilibrium case, the PCM response matrix $\mathcal{Q}$ depends on the dielectric constant at optical frequency (ϵ_{opt}), whereas in the equilibrium case it depends on ϵ.

A significant part of solvent effect on the excited-state energies is recovered by LR approaches using MO orbitals computed in solution (and, thus, including the polarization due to the solvent reaction field) [83]. However, since the exact excited-state electron density is never computed, all the solvent contributions depending on the variation of the multipole moment upon excitation are missing in LR computations. An additional PCM correction is instead introduced which depends on the ground–excited state transition density [83]. As a consequence, the treatment of dynamical solvent effects is completely different with respect to that made by SS-PCM (in Eq. 1.18 explicit reference is made to the excited-state density). Furthermore, in the LR-PCM method the ground state is thus always fully equilibrated with the solvent degrees of freedom. As a consequence, in the nonequilibrium case the solvation contribution to the emission energy is computed as

$$\Delta G_{\mathrm{em}}(\mathrm{LR}) = \mathcal{G}^{(2)}_{\mathrm{neq}}(\mathrm{LR}) - \mathcal{G}^{(1)}_{\mathrm{eq}} \tag{1.26}$$

whereas for long living excited state it is computed as

$$\Delta G_{\mathrm{em}}(\mathrm{LR}) = \mathcal{G}^{(2)}_{\mathrm{eq}}(\mathrm{LR}) - \mathcal{G}^{(1)}_{\mathrm{eq}} \tag{1.27}$$

that is, in standard LR-PCM the equilibrium solvation energy for the ground state is used in both cases, making this method not suitable to an accurate treatment of the solvent effect on the emission process.

1.5 COMPUTING SPECTRA: THEORY

1.5.1 Choice of Functional

As anticipated above, results of the many computational studies of excited states exploiting TD-DFT have clearly highlighted that the accuracy of the computed vertical excitation energy (VEE) remarkably depends on the adopted functional. Several studies show that the local density approximation (LDA) (the exchange/correlation energy is a function of only the local value of the electron density) underestimates the VEE of valence transitions in organic molecules [89]. In particular, there is a marked deterioration of the results for high-lying bound states [51–58].

Better results are obtained by functionals exploiting the generalized gradient approximation (GGA, the functional depends on both the density and its gradient), such as BLYP [90], PBE [91], or HCTH [92]. These functionals have limited computational requirements, they can be easily implemented in ab initio molecular dynamics methods like Car–Parrinello, and in some systems, such as metals, they can provide rather reliable excitation energies. However, a huge number of computational studies indicate that they are usually outperformed by their "hybrid" analogues, that is, functionals, including a fraction of "exact" exchange, computed at the Hartree–Fock level of theory. The most popular hybrid functionals, such as B3LYP [93] or PBE0 [94–96], contain, in each point of the space, the same percentage of HF exchange, and they can thus be labeled as "global hybrids". These functionals, especially B3LYP, are surely the most commonly used functionals not only for ground-state DFT but also for TD-DFT excited-state calculations [53].

Local hybrid (LH) functionals are characterized by a mixing of HF exchange that depends on the spatial electronic coordinate (as LH-BLYP) [97]. Finally, range-separated hybrids (RSHs) use a growing fraction of exact exchange as the interelectronic distance increases, giving a long-range correction (LC) to the original DFT scheme [72, 73]. Functionals such as CAM-B3LYP [72] or LC-ωPBE [73] are representative of this class of functionals. Functionals that depend explicitly on the semilocal information in the Laplacian of the spin density or of the local kinetic energy density also have been developed [98]. Such functionals (see, e.g., the functionals of the M05 or M06 family) [51] are generally referred to as meta-GGA functionals.

Obviously, a thorough comparison among the performances of the different functionals is outside the scope of the present chapter (see refs. 51–58 for recent reviews). On the other hand, it is possible to draw some general guidelines for the selection of the density functional to use in TD-DFT calculations, summarizing the requirements for an "optimal" density functional. A first critical feature of a functional concerns the philosophy underlying its development. According to a first broad school of thought, once an appropriate functional form has been selected, the functional is heavily parameterized by reference to experimental data or data from explicitly correlated ab initio calculations [92]. Alternatively, the exact properties of the functional (determined to fulfill a series of physical conditions) can be used to determine both its structure and, eventually, the parameters in its functional form.

Based on our experience in the field, we think that a density functional with a small number of (ideally zero) adjustable parameters, and thus tailored according to this latter approach, would be preferable. Although it can deliver worse performances than heavily parameterized functionals in several cases, it is safer for studying systems that could not belong to the class of compounds used in the parameterization procedure.

A suitable functional should obviously also provide reliable results, namely (i) accurate ground-state geometries/vibrational frequencies, (ii) balanced description of valence and Rydberg states, (iii) balanced description of bright and dark excited states, (iv) good excited-state geometries/vibrational frequencies, and (v) a correct description of charge transfer states.

It is clear that a "perfect" functional fulfilling all the above requirements probably does not exist. Several different analyses have appeared in the literature comparing the performance of different functionals, sometimes with contradictory results [51–58]. Actually, it is necessary to pay a lot of attention when analyzing the studies assessing the performance of the different functionals (or, obviously, of different QM methods), especially when they are based on comparison with experimental results. In fact, (i) the VEE is not an observable and it does not necessarily coincide with the band maximum; (ii) as a consequence, absolute error is not necessarily the most significant property; (iii) reproducing trends (i.e., substituent effect) can be more important; and (iv) most of the experimental results are obtained in solution but most of the computational studies are performed in vacuo.

However, it is nowadays well assessed that hybrid functionals usually outperform nonhybrid ones and that the most commonly used hybrid functional, B3LYP, is not the best one (vide infra) [51–58].

Our previous experience suggests that the PBE0 hybrid functional is a "well-balanced" functional, usually providing very accurate results. In PBE0 the amount of exact exchange has been determined in order to fulfill a number of physical conditions without resorting to any fitting procedure [94]. PBE0, obeying both the Levy condition [99] and the Lieb–Oxford bound [100], provides a fairly accurate description of the regions characterized by a low electron density but, at the same time, by a high value of the electron density gradient. A reliable description of this region is important not only for a system dominated by dispersions interactions (e.g., van der Waals complexes) but also for higher lying excited states, as, for example, Rydberg states. For these reasons, TD-PBE0 excitation energies are, on the average, more accurate than those provided by other commonly used hybrid functionals, such as B3LYP [96]. The Becke exchange functional, not obeying the Levy condition [99] or the Lieb–Oxford bound [100], exhibits an incorrect asymptotic limit. Despite the absence of adjustable parameters, besides providing a reliable description of the ground-state properties of several classes of compounds, TD-PBE0 results have shown an overall degree of accuracy comparable with that of the best last-generation functionals in the description of both bright and dark excitation and both valence and Rydberg states [53–58]. Furthermore, the vibrational analysis performed on the ground of TD/PBE0 results (excited-state minima geometry and vibrational frequencies) turned out in remarkable agreement with the experimental indications for several classes of compounds [45–50].

On the other hand, PBE0 (like all the standard density functionals) exhibits important failures in describing zero-overlap CT transitions. In these cases, a check using purposely tailored functionals (CAM-B3LYP, M06-2X, LCω-PBE) is highly recommended.

1.5.2 Choice of Basis Set

As already anticipated, one of advantages of using TD-DFT is that this method does not exhibit any dramatic dependence on the size of the basis set. For valence transitions, many studies indicate that a medium-size basis set (valence double-zeta or triple-zeta adding polarization and diffuse functions) provides VEE close to convergence [53–58].

Based on our experience, the small 6-31G(d) basis sets provide sufficiently accurate equilibrium geometries and vibrational frequencies, and 6-31G(d) energy ordering is usually qualitatively correct, but for Rydberg states. Although the computed trend depends on the kind of transition considered, the VEE obtained at the 6-31+G(d,p) level are close to convergence (representing a good compromise between accuracy and computational cost). Finally, 6-311+G(2d,2p) results can be considered converged in the great majority of the systems.

The above considerations do not hold when studying excited states with Rydberg character: These transitions require more extended basis sets [6-31+G(d,p) is the minimal basis set possible], the inclusion of diffuse functions is mandatory, and their energies converge more slowly with the size of the basis set.

Analogously, the study of charged species, especially anions, in their electronic excited states requires, on average, more extended basis sets than that of their neutral counterpart. In this case, for example, the energy ordering obtained at the 6-31G(d) level is often misleading.

Particular attention has to be paid to the basis set adopted in PCM/TD-DFT calculations. The PCM cavity radii most commonly adopted have been parameterized in order to reproduce solvation energies (i.e., a ground-state property) at a specific level of theory [HF/6-31G(d), HF/6-31+G(d,p) for the anions, PBE0/6-31G(d), etc.] [101]. When using different basis sets, different results can be obtained, especially when thinking that VEE involves virtual molecular orbitals, which are usually more diffuse than the occupied ones and whose behavior "optimal" radii are likely different with respect to those used for the ground state. To compute the solvent effect on the excited states, the safer procedure is using a basis set not too large, similar to that used for the radii optimizations 6-31G(d), 6-31+G(d,p) for charged species.

1.5.3 Choice of Solvation Model

The two basic choices concern (i) the solvation model and (ii) the method to use. As discussed above, a continuum model such as PCM offers several advantages over purely supramolecular methods. On the other hand, PCM is expected to provide a good estimate of the electrostatic contribution to the solute–solvent interaction, whereas less accurate results can be obtained when dealing with nonpolar or

hydrogen-bonding solvents. In the former case, the nonelectrostatic contribution (dispersion interactions, electronic repulsion) to the solute–solvent interaction is larger than the electrostatic one. Solvent shift in a nonpolar solvent, for example, can depend on the variation of the polarizability associated with the electronic transition more than on the dipole moment shift. Interesting attempts to treat this kind of problem within the framework of PCM/TD-DFT calculations have been made [102], but it cannot be taken for granted that standard calculations are able reproduce solvent effect in nonpolar solution (dielectric constant <4) or when dealing with nonpolar solutes. For hydrogen-bonding solvents, as anticipated above, the solute–solvent interactions can be highly directional and have a strongly molecular nature, that is, that cannot be properly described by simple electrostatic interactions. Consider, for example, the hydrogen bond formed by a water molecule and the lone pair of a carbonyl group. As we shall verify when reporting the results of our study on uracil, an electronic transition involving the carbonyl lone pair would significantly perturb the hydrogen bonds in which it participates. An accurate estimate of the effects of the electronic transition to the hydrogen bond interaction can be obtained only at the QM level, that is, explicitly including the solvent molecule in the computational model. Although PCM alone can provide useful hints on the solvent shift in hydrogen-bonding solvents, an accurate determination of the absorption and emission spectra requires that the most important solute–solvent interactions, say, the first solvation shell, are considered in the calculations by means of a mixed discrete-continuum approach [81]. Although there is no general rule concerning the number and geometry of the solvent molecules to be considered, as we shall see in the next sections, combining chemical intuition with experimental results, it is relatively easy to design a computational model able to provide accurate results.

As discussed above, PCM/TD-DFT being a reference method, it is still necessary to choose between LR-PCM/TD-DFT and SS-PCM/TD-DFT calculations. It is however important to remind that several of the following considerations are valid for many of the LR-PCM and SS-PCM methods.

LR-PCM/TD-DFT is surely the simplest and fastest method for computing absorption and emission energies in solution, its computational cost being only marginally larger than the corresponding gas-phase TD-DFT calculation. The availability of LR-PCM/TD-DFT analytical gradients gives relatively easy access to excited-state minima, other excited-state properties as the multipole moment, as well as all the different population analyses available for the ground state. Vibrational frequencies in solution can be obtained by numerical second derivatives of the energy, increasing their computational cost. The $6 \times N$ PCM/TD-DFT single-point calculations are indeed necessary to obtain the vibrational frequencies of a molecule containing N atoms. Furthermore, it is necessary that the procedure is performed with a lot of caution when in the presence of two close-lying excited states.

The results of a large number of studies indicate that LR-PCM is able to provide a fairly accurate estimate of the VEE in solution, especially for what concerns the bright excited states [53–58]. On the other hand, LR-PCM has been shown to overestimate solvent effects on the intensities, especially at the EQ level [85, 86]. The two most significant limitations of LR-PCM concerns (i) the treatment of the emission process

(and in general the dynamical solvation effect) and (ii) the study of the electronic transitions involving a substantial electron density shift [85, 86].

For the emission process, we recall that in LR-PCM calculations solvent degrees of freedom are always equilibrated with the ground-state density and in general, this method provides a less rigorous treatment of dynamical solvent effect than SS-PCM. For example, the solvent reorganization energy (λ), that is, the difference between the energy of a state in the NEQ and in EQ limits, is not correctly computed by LR-PCM. In this method λ is proportional to the square of the transition dipole moment: It is thus larger for bright transitions, being zero for dark states. Furthermore, in LR-PCM the excited-state energy does not exhibit any dependence on the excited-state dipole moment, and thus the energy of the excited states with a large dipolar character (e.g., the CT transitions) is significantly underestimated, especially at the EQ level [85, 86].

On the other hand, most of the above deficiencies are not present in SS approaches, as SS-PCM/TD-DFT, which instead gives a balanced description of strong and weak electronic transitions (see also the results reported below). Several studies (see below) indicate that SS-PCM/TD-DFT provides accurate estimates of dynamical solvent effects on the absorption and emission processes, of solvent reorganization energy, and thus of inhomogeneous broadening. For example, in SS-PCM/TD-DFT λ is indeed proportional to the square of the dipole moment shift associated with the transition, which is indeed expected to be the leading term in a polar solvent [85, 86].

Unfortunately, SS-PCM/TD-DFT excited-state analytical gradients are not available. Furthermore, SS-PCM has an iterative implementation which not only increases the possibility of convergence failures but would also make geometry optimizations rather cumbersome.

An effective strategy is thus complementing the results of LR-PCM/TD-DFT geometry optimizations by single-point SS-PCM calculations. In any case, notwithstanding the above caveat, in many systems a good agreement between LR-PCM/TD-DFT results and experimental absorption and emission spectra has been found [53–58, 78]. It has indeed been shown [83] that at the zero order, related to the interaction with the slow solvation degrees of freedom, LR and SS approaches are identical [83].

It is necessary, finally, to comment on another factor potentially affecting the computed spectral parameters, that is, the cavity radii [88]. As we have anticipated above, the solute cavity within PCM has built as envelope of spheres centered on the atoms or atomic groups. Different parameters are involved in the building of the cavity; one of the most important obviously is the radii associated with each sphere, which rules the volume of the cavity and, thus, the distance between the atoms and the cavity surface. It is well known that the computed properties depend on the adopted atomic radii, and this is obviously true also for the excited-state energies. Both SS-PCM and LR-PCM results depend on the cavity model adopted, especially on the radii used. Additional studies are necessary to shed light on this latter point. Several studies indicate that using the cavity models developed for ground-state computations usually provides fairly accurate results [53–58]. However, this feature has to be considered with particular attention when comparing different kinds of transitions. Furthermore, since the choice of the cavity affects the relative energy of the transition, some critical features (e.g., the presence of a crossing) can depend on the cavity.

1.6 COMPUTING SPECTRA: APPLICATIONS

Before examining in detail the results of some TD-DFT applications to the computation of the spectra, it is useful to provide some hints about the expected accuracy of this method and of the different functionals. Although the huge number of studies makes it almost impossible to give a comprehensive picture, very interesting indications are provided by the very careful studies of Jacquemin, Adamo, and colleagues, performed a systematic comparison among the experimental absorption spectra of several classes of organic dyes of industrial interest (azobenzene, anthraquinone, indigos, arylethenes) and the VEE computed at the TD-DFT level using different density functionals [53–58].

As expected, their analysis shows that the performances of TD-DFT, in general, and of the different functionals depend on the class of compounds examined. For 189 anthraquinone derivatives solvated in various media (CH_2Cl_2, methanol, and ethanol), the mean absolute errors (MAEs) are 0.10 eV for both PBE0 and B3LYP [53]. For 304 indigoid derivatives, PCM-TD-PBE0/6-311+G(2d,p)//PCM-PBE0/6-311G(d,p) calculations provide excitation energies with a MAE limited to 0.04 eV with respect to the experimental band maxima [53].

Including other class of compounds in the analysis, such as azobenzene, coumarins, diaryl-ethenes, and diphenylamine derivatives, does not change significantly the picture: The best performances are delivered by PBE0, with an average absolute deviation limited to 0.14 eV/22 nm, which has been proposed to be the expected PCM/TD-PBE0 accuracy for low-lying excited states of conjugated organic compounds. The second best approach, CAM-B3LYP, suffers larger deviations (0.26 eV/38 nm) but appears particularly well suited for studying dyes with a very delocalized excited state. Furthermore, CAM-B3LYP provides a very good estimate of substituent effect on the absorption spectra [54].

When class of compounds that are known to be ill-treated by TD-DFT, for example, cyanine, are included in the set of the experimental data ($\sim$500 compounds and more than 700 excited states), the average error of TD-PBE0 VEE increases up to 0.24 eV, and a similar value is obtained when the comparison is made with the best theoretical estimates computed for a smaller set of compounds in the gas phase (104 singlet state). In any case, such a value is an average between that expected for electron transitions with a monodeterminantal nature, for which PBE0 (and other hybrid functionals including 20/30% of HF exchange) is remarkably accurate (expected error $\sim$0.15 eV), and those with a strong multideterminantal nature (e.g., cyanine, triphenylmethane, and acridine derivatives) for which TD-DFT is inadequate [54].

Interestingly, the analysis of Jacquemin et al. [54] shows that the accuracy of PBE0 (and of other hybrid functionals containing a similar percentage of HF exchange) for $n \rightarrow \pi^*$ transitions is even larger than that found for $\pi \rightarrow \pi^*$ transitions, the MAE with respect to the experiments being close to zero. This results, as highlighted by Jacquemin et al. is probably due to the more local character of $n\pi^*$ transitions in the examined set.

Rydberg excitations are another class of transitions that have been traditionally considered "not reliably" treated at the TD-DFT level. Actually, several studies

have shown that, besides the use of at least one diffuse function of the heavy atoms, the accuracy of TD-DFT calculations dramatically depends on the adopted functional. Indeed, in order to correctly describe low-density/high-density gradient regions as those involved in Rydberg excitations, it is necessary to use an exchange-correlation functional exhibiting a correct asymptotic behavior:

$$\lim_{r \to \infty} v_{xc}(r) = -\frac{1}{r} \tag{1.28}$$

When functionals, such as PBE0, fulfilling the above condition are employed, fairly accurate VEEs are obtained for Rydberg excitations, the MAE being <0.4 eV for several organic compounds [54].

For metallo-organic systems, to the best of our knowledge, no such systematic comparisons between TD-DFT and experimental results exist in the literature. Accurate results have been obtained on several porphyrin-like metal complexes [103]. TD-PBE0 delivers reliable results in the study of several Ru–polypyridine complexes, although its accuracy is lower than that found for organic molecules (errors in the range 0.15–0.4 eV) [53]. Standard functionals such as B3LYP have often been successfully applied to interpret the spectra of Ru–dye complexes of potential interest for the development of solar cells [104]. On the other hand, studies of $[Ni(H_2O)_6]^{2+}$ complexes show that TD-B3LYP are not fully reliable, even qualitatively, due to the lack of transitions of double-excitation character and the wrong treatment of CT transitions (the energy of the LMCT transitions is significantly underestimated) [105]. In summary, additional studies are probably necessary to assess the general reliability of TD-DFT for the study of the visible spectra of metallo-organic systems, since the quality of the results can depend on several additional factors (proper inclusion of relativistic effects, pseudopotential employed, spin–orbit coupling) with respect to those examined for organic molecules.

Both for organic and metallo-organic systems, studies in the literature show that TD-DFT, also employing a standard hybrid functional such as PBE0, can provide a remarkably accurate description of transitions with partial CT character (see also Section 1.6.1.2). In fact, we remind the reader that the failures of TD-DFT calculations are usually associated with long-range CT between two partners whose molecular orbitals have a vanishing overlap. On the other hand, CT transitions in which donor and acceptor have a small but nonzero overlap (e.g., the metal to ligand charge transfer (MLCT) transitions in several inorganic complexes) can be treated in a fairly accurate way without resorting to long-range corrected functionals [53].

1.6.1 Selected Examples

To better illustrate the general concepts summarized above, it can be useful to make explicit reference to the calculation of the vertical absorption and emission energies of some representative compounds in different environments. Based on previous

experience, we discuss in some detail the results obtained in the study of nucleic acid components and one of the most used solvent probes, coumarin C153.

1.6.1.1 Bases of Nucleic Acids

Uracil in Gas Phase Absorption of UV–vis radiation by DNA and its constituents is a phenomenon of fundamental biological interest. Indeed, since many DNA photolesions are triggered by the population of singlet excited electronic states, the availability of a fast radiationless decay channel is very important to life [106]. As a consequence, the excited states of the nucleic acid bases (nucleobases) have been thoroughly investigated by many experimental and computational studies, both in the gas phase and in solution, providing several indications of the performances of the different computational approaches. Uracil (see Figure 1.1) is probably the nucleobase examined more in detail [107–123]. Experiments reveal the presence of a strong absorption band at ∼4.8–5.0 eV (depending on the solvent), and computations ascribe this feature to a π/π^* transitions (hereafter $S\pi$), which mainly corresponds to a HOMO → LUMO excitation [107]. Different computational methods agree in predicting that $S\pi$ is not the lowest energy excited state in the FC region: Indeed, an underlying dark state is predicted, with $n\pi^*$ character (hereafter Sn), which mainly arises from the excitation of an electron from the lone pair (HOMO-1) of the C4–O8 carbonyl group (see Figure 1.1) to the π^* LUMO [108]. The energy difference between Sn and $S\pi$ is thus another quantity of relevant interest, especially when

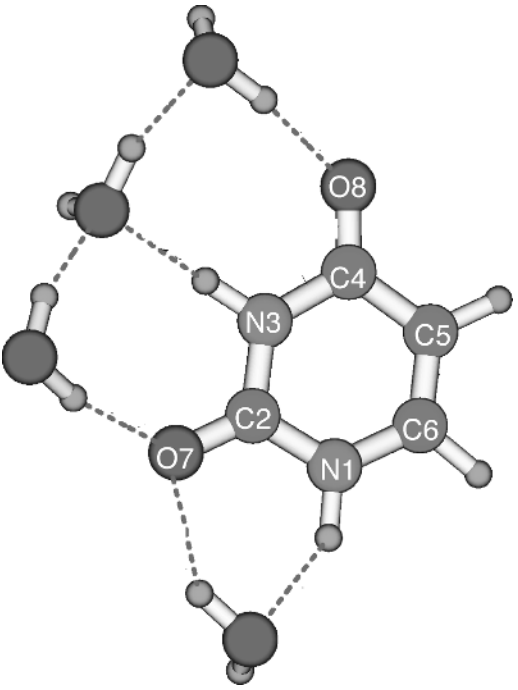

Figure 1.1 Schematic description (and atom labeling) of uracil·4 H_2O model.

thinking that, according to both experiments and computations, a significant $S\pi \rightarrow Sn$ population transfer is possible [109, 110].

A thorough study of the uracil in the gas phase has been performed by Matsika et al., which compared the results obtained by the equation-of-motion coupled-cluster and multireference configuration interaction methods with those provided by other computational methods [108]. The completely renormalized EOM-CCSD with the noniterative triples CR-EOM-CCSD(T) method, based on the methods of moments of coupled-cluster equations, used with the aug-cc-pVTZ basis set, predicts that $S\pi$ and Sn VEEs are 5.25 and 5.00 eV, respectively. MRCI(12,9)/aug-ANO-DZ calculations, including the Davidson correction (the expansion consists of about 330 million configuration state functions), predicts that $S\pi$ VEE is 5.32 eV, whereas, at this level of theory, the authors did not succeed in obtaining the Sn energy due to technical difficulties. CASPT2(14,10)/6-31G(d,p) calculations provide similar indications, $S\pi$ VEE = 5.18 eV and Sn VEE = 4.93 eV. Inspection of Table 1.1 clearly shows that the results provided by the TD-PBE0 method are extremely close to those obtained by using much more computationally demanding methods and much more accurate than other ab initio methods as CC2. The only significant discrepancy with respect to CCSD(T) predictions concerns the energy difference between $S\pi$ and Sn, which is 0.2 eV larger in PBE0, and, in this respect, this prediction looks more consistent with the experimental indications in water (vide infra). Furthermore, TD-PBE0 results are much less dependent on the basis set size than those provided by EOM/CCSD(T) or CASPT2. These two latter methods also exhibit a marked dependence on the size of the active space included in the calculations. In the wave function method these features make it much more difficult to treat large-size systems, for which the use of

Table 1.1 Comparison between VEE Computed for Two Lowest Energy Excited States of Uracil Using Different Computational Approaches

Method	Basis Set	$n\pi^*$	$\pi\pi^*$
CR-EOM-CCSD(T)	aug-cc-pVTZ	5.00	5.25
CR-EOM-CCSD(T)	6-31G(d)	5.19	5.65
EOM-CCSD	aug-cc-pVTZ	5.23(0.00)	5.59(0.20)
CASPT2(14,10)	6-31G(d,p)	4.93(0.00)	5.18(0.20)[a]
MS(3)-CASPT2(12,10)[b]	6-31G(d)	5.16(0.00)	5.52
CASPT2//CASSCF(14,10)[c]	ANO		5.02
MRCISD+Q(12,9)	aug-ANO-DZ	not conv	5.32
CC2	TZVP	4.91	5.52
PBE0	6-311+G(2d,2p)	4.81(0.00)	5.26(0.14)
PBE	6-311+G(2d,2p)	4.00(0.00)	4.76(0.06)
LC-ωPBE	6-311+G(2d,2p)	5.06(0.00)	5.40(0.18)
B3LYP	6-311+G(2d,2p)	4.68(0.00)	5.15(0.13)
CAM-B3LYP	6-311+G(2d,2p)	5.08(0.00)	5.40(0.18)
M052X	6-311+G(2d,2p)	5.02(0.00)	5.51(0.20)

[a] From ref. 111.
[b] From ref. 112.
[c] From ref. 113.

large basis sets and active spaces is rather cumbersome. Inspection of Table 1.1 shows that, on average, PBE0 exhibits the best performances among the functionals examined. Long-range corrected functionals, CAM-B3LYP or LC-ωPBE, overestimate the VEE of $S\pi$ by at least 0.2 eV. A pure density functional such as PBE significantly underestimates both $S\pi$ and *Sn* VEE. B3LYP provides similar results as PBE0, but *Sn* VEE exhibits a larger discrepancy with respect to the most accurate WF-based methods than that provided by PBE0.

Interestingly, the maximum of the absorption band of uracil in the gas phase is 5.08 eV, that is, 0.1–0.2 eV red shifted with respect to the "best" computational estimates. In any case, it is important to remember that the shape and maximum of the experimental absorption band can be significantly modulated by vibrational and vibronic effects.

Uracil in Water Solvent noticeably affects the energy of the excited states and their relative stability. For example, the absorption band maximum of uracil in water is $\sim$0.25 eV red shifted with respect to the vapor phase [114]. *Sn* is known to be significantly destabilized in water, and solvent has been shown to modulate the excited-state dynamics in uracil derivatives [107, 115].

Our studies in the field have already unambiguously shown that proper description of solvent shifts of uracil excited states in aqueous solution requires that both bulk solvent effect and solute–solvent hydrogen bond interactions have to be considered [107, 109, 112, 115, 116]. As shown in Table 1.2, in fact, inclusion of bulk solvent effects by the PCM model decreases by 0.1 eV $S\pi$ VEE and increases by 0.35 eV that of *Sn*. When four water molecules of the first solvation shell are included in the model (see Figure 1.1), and gas-phase calculations provide similar trends. When both effects are considered, *Sn* is strongly destabilized (by $\sim$0.5 eV), whereas the computed solvent red shift for $S\pi$ (0.2 eV) approaches that predicted by the experiments ($\sim$0.25–0.3 eV). Inclusion of water molecules is particularly important to correctly reproduce the solvent effect on *Sn*: This electronic transition involves the transfer of an electron from the oxygen LP, which can potentially act as hydrogen bond acceptors, toward the more diffuse π^* molecular orbital, leading to a decrease of the solute–solvent hydrogen bond strength.

The VEEs of uracil in water solution have also been studied by other approaches [117–120]. MRCI/cc-pVDZ/MM calculations (considering 257 water molecules as fixed charges, whose position is averaged by means of MD simulation) predicts that in water $S\pi$ VEE is red shifted by $\sim$0.05–0.1 eV and *Sn* VEE blue shifted

Table 1.2 Comparison between the VEE Computed for Two Lowest Energy Excited State of Uracil Using Different Models

Excited State	Gas Phase	Gas Phase + 4 H_2O	Water PCM	Water PCM + 4 H_2O
Sn	4.81(0.00)	5.11(0.00)	5.15(0.00)	5.32(0.00)
$S\pi$	5.26(0.14)	5.19(0.15)	5.16(0.20)	5.10(0.20)

Note: PBE0/6-311+ G(2d,2p)//PBE0/6-31G(d) calculations.

by ∼0.4 eV with respect to the gas phase [117]. The use of the fragment molecular orbital multiconfigurational self-consistent field (FMO-MCSCF), which partially includes quantum effects in the description of the solute–solvent interactions, provides solvent shifts closer to the experimental estimates and to our computational results: for $S\pi \sim -0.15/-0.18$ eV, for $Sn \sim +0.42/+0.47$ eV. EOM-CCSD(T)/MM calculations provide a $+0.44$ blue shift for Sn and a $+0.05$ blue shift for $S\pi$, and this latter result is in qualitatively disagreement with experiments. Using Monte Carlo simulations on 200 water molecules to generate solvent configurations around uracil, which have then been used for intermediate neglect of differential overlap (INDO) excited-state calculations, indicate $+0.5$-eV and -0.19-eV solvent shifts for Sn and $S\pi$, respectively [119]. On the balance, it seems that a mixed discrete–continuum approach, notwithstanding by far the computationally less demanding, provides the most accurate predictions. On average, we can thus estimate that, when going from the gas phase to water, Sn is destabilized by ∼0.7 eV with respect to $S\pi$. As a consequence, in the FC region Sn is less stable than $S\pi$ by ∼0.2 eV only. Such a difference is fully compatible with the partial $S\pi \rightarrow Sn$ population transfer evidenced by time-resolved experiments for uracil in water [109, 110]. On the other hand, if we assume that in the gas phase Sn is less stable than $S\pi$ by ∼0.25 eV only (as predicted by EOM-CCSD(T) or CASPT2 calculations), the energy difference in water would be ∼0.5 eV, a value which would make the population transfer much less likely. Those considerations clearly show that careful study of the solvent effect is mandatory in order to use computational results obtained in the gas phase to study processes occurring in solution or just to assess the reliability of a given computational method.

Actually, our mixed discrete–continuum model is not limited to the study of UV–vis spectra, but it has been already successfully employed to model solvent effects on several different spectral properties, such as electron paramagnetic resonance (EPR) hyperfine coupling constants, nuclear magnetic resonance (NMR) chemical shifts, and so on [45, 121].

The only point not unambiguously defined in our model concerns the number and position of the solvent molecules to be explicitly included in the calculations. Although it is not possible to define strict and general rules, a suitable combination between experimental and computational indications and chemical intuition in most of cases allows for obtaining reliable results. For uracil in water, for example, NMR experiments indicate that no water molecule is strongly bonded to C5 and C6 carbon atoms and that O7 and O8 are coordinated by two and one water molecules, respectively [122]. Car–Parrinello dynamics suggest that the first coordination shell of uracil (up to 2.5 Å) is formed by six water molecules, four in the molecular plane (as in Figure 1.1) and two more or less perpendicular to it [123]. Although a full description of the first solvation shell in solution requires, of course, a proper dynamic treatment, a number of studies have confirmed that the PCM is able to accurately account for the effect of water molecules that are more distant and/or not directionally bound to the carbonyl oxygen lone pairs. The model depicted in Figure 1.1 thus appears a reasonable guess, to be further refined by means of PCM geometry optimizations. Furthermore, our previous experience suggests that inclusion of bulk solvent effects by means of PCM significantly decreases the dependence of the

computed VEE on the "exact" coordination geometry of the first solvation shell, and, in many cases, also on the number of solvent molecules considered. Geometry arrangements that in the gas phase are predicted to have significantly different energy and/or spectral properties appear almost isoenergetic at the PCM level, which is able to correctly reproduce the energetic effect of the outer solvation shells.

Guanine in Water at Strongly Acidic pH According to our model, in both ground, and excited-state geometry, optimizations, the first solvation shell is fully optimized, that is, it is treated like solute degrees of freedom. Since outer solvation shells are not included in our calculations, this choice is expected to overestimate the conformational flexibility of the water molecules of the cybotactic region, suggesting that particular attention has to be paid when investigating dynamical solvation effects. In some cases the number of solvent molecules included in the model can also affect the computed excitation energies. An example of this feature is provided by our recent study of the excited-state dynamics of guanine monophosphate (G) [124]. In this study it is shown that protonation of nitrogen N7 (see Figure 1.2) in strongly acidic conditions noticeably affects the behavior of the lowest energy bright state (L_a). We have compared the results obtained by including five (G-Wa5) or 6 (G-Wa6) water molecules in our computational model. While for the neutral compound no minimum is found in the path leading from the FC to the CoI with S_0, for the protonated

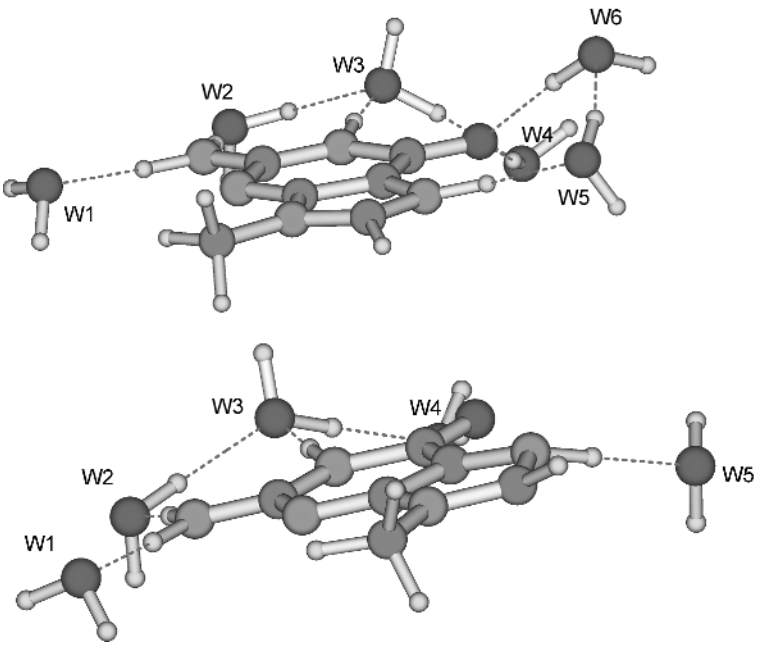

Figure 1.2 Schematic description of the minima of the lowest excited state of 9-methylguanine in water in strongly acidic conditions, computed in water at the PCM/TD-PBE0/6-31G(d) level by using a model including five (up) or six (down) water molecules.

compound a minimum is found, where the N7 and C8 hydrogens are out of the molecular plane (see Figure 1.2), with concomitant motion of water molecules in the first solvation shell. Interestingly, the out-of-plane distortion is larger for the model with G-Wa5, since in G-Wa6, due the presence of an additional hydrogen bond between the solvent molecules of the first solvation shell, the motion of the water molecule hydrogen bonded to the N7-H group is more restrained. The different geometry of the excited-state minimum is obviously mirrored in the computed emission energy, which is larger by $\sim$2200 cm^{-1} for G-Wa5, since distortion from planarity significantly destabilizes S_0. It is thus clear that, especially for excited-state geometry optimizations, there are situations where different choices of the solvation shell can noticeably affect the computed spectra. On the other hand, it is important to remind that both G-Wa5 and G-Wa6 models are able to reproduce the effect of the protonation on the emission spectra, disclosing the underlying chemical–physical effects. In fact, experiments show that the Stokes shift is significantly larger (by $\sim$4000 cm^{-1}) for the protonated compound, in line with computational predictions.

1.6.1.2 Coumarins The results obtained in the study of coumarin, especially that of C153, allows getting additional insights on the treatment of non-hydrogen-bonding solvents. In coumarins (see Figure 1.3), the $S_0 \rightarrow S_1$ transition has a $\pi \rightarrow \pi^*$ character, and it essentially corresponds to a HOMO $\rightarrow$ LUMO transition [46, 47]. However, while the HOMO is delocalized on the whole molecule, with significant contribution by the π orbitals of the "central" benzene ring and of the nitrogen atom, the LUMO is mainly localized on the "quinone like" terminal ring with significant contribution of the π^* orbital of the carbonyl group. As a consequence, the $S_0 \rightarrow S_1$ transition has a partial intramolecular charge transfer character (from the nitrogen atom to the carbonyl group), and S_1 has a partial zwitterionic character (with the nitrogen

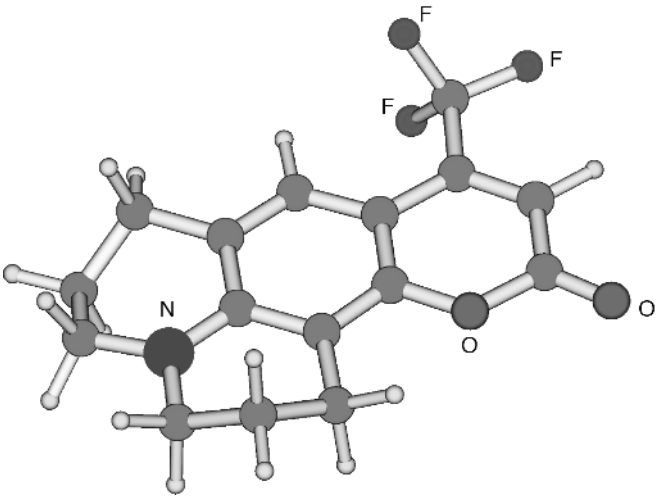

Figure 1.3 Schematic drawing of anticonformer of coumarin C153.

atom and the oxygen of the carbonyl group bearing a formal positive and negative charge, respectively). This results in a significant solvent shift of this transition, which, coupled to the molecular rigidity, makes coumarin and, in particular, C153 ideal tools for investigating the different solvation rates by time-resolved spectroscopic techniques, being the most used "molecular probes" of crucial dynamical aspects of solvation [125, 126].

Starting our analysis from the gas phase, the picture of the C153 excited states obtained at the TD-PBE0 level is in remarkable agreement with the experimental one. The 0–0 transition energies computed in the gas phase by the PBE0 functional for the nearly isoenergetic syn and anti isomers of C153 (25,680 and 25,660 cm^{-1}) are indeed in almost quantitative agreement with the experimental values (25,898 and 25,710 cm^{-1}, respectively) [127]. The calculated values for the oscillator strength (0.36 and 0.37, respectively) match their experimental counterpart (0.37) [128]. Finally, PCM/TD-PBE0 calculations predict that in both dimethyl sulfoxide (DMSO) and cyclohexane the dipole moment shift ($\Delta\mu$) associated with the electronic transition is $\approx$6.0 D (see also ref. 85). This value is in good agreement with the estimates based on electroabsorption experiments [129] and slightly underestimated with respect to the experimental determination in the gas phase [130].

The very good agreement between experimental and computational results could seem at a first sight surprising due to the partial CT character of the S_0–S_1 transition. On the other hand, the C153 lowest energy transition involves only partial intramolecular CT and can be correctly treated by hybrid functionals, as shown by the results obtained on dimethylaminobenzonitrile [131]. In this respect, it is noteworthy that for C153 conventional GGA functionals provide much less accurate results than their hybrid counterpart: For instance, the PBE functional [91] provides gas-phase 0–0 transition energies of 19,845 and 19,931 cm^{-1} for the syn and anti isomer, with a significant underestimation ($\approx$6000 cm^{-1}) with respect to experimental results.

Comparison between vertical excitation and emission energies computed at the SS-PCM/TD-PBE0 and LR-PCM/TD-PBE0 levels confirms that the former method is significantly more accurate than the latter, especially for the emission energy in DMSO and, consequently, for estimating both the solvatochromic shift and the Stokes shift in DMSO. In fact, the predicted Stokes shift in DMSO, which is underestimated by 1200 cm^{-1} at the SS level, is underestimated by 3000 cm^{-1} at the LR level and, in the same way, the solvatochromic effect DMSO–cyclohexane for fluorescence (overestimated by 400 cm^{-1} at the SS level) is underestimated by 2200 cm^{-1} at the LR level [47]. These results confirm that it is important to resort to SS-PCM single-point calculations for an accurate evaluation of the emission process and of the dynamical solvent effects. On the other hand, the very good agreement between the computed and experimental lineshapes supports the general accuracy of the equilibrium structures and vibrational frequencies provided by LR-PCM/TD-DFT calculations [45–50]. From the general point of view, our studies on coumarins (not only on C153 but also on other coumarin derivatives) [86] shows that, as already stated, solvent models based on a polarizable continuum, at least when dealing with non-hydrogen-bonding solvents, are able to capture the "physics" of time-dependent phenomena in solution.

1.6.2 Dealing with Supramolecular Interactions: Optical Properties of DNA

In the examples considered until now, we have tackled the study of a medium-size molecule (a single chromophore) in solution. The theoretical/computational framework we have outlined can be rather easily applied to other several systems, such as, for example, a chromophore embedded in a protein. In this latter case, the chromophore can be treated by using the methods described above, and the only difference concerns the inclusion of environmental effects. Mixed QM/MM methods are indeed usually more suitable than continuum models for treating highly nonisotropic environments as proteins [132]. Many processes of biological or technological interest, however, depend on multiple chromophores arranged in supramolecolar structures. The optical properties of those systems are traditionally treated by semiempirical methods, where the interaction among the chromophores is included at a simplified level (e.g., by considering the dipolar/dipolar coupling between the excited-state transitions in the isolated chromophore). However, it is nowadays possible to attain a fully quantum mechanical description of the optical properties of complex supramolecular structures, as shown by the results obtained on DNA single and double strands [133–136].

The computation of nucleic acid UV–vis spectra is an ideal test case for theoretical and computational models. Not only are a large number of experimental results (also time resolved) available [106], but, since the DNA monomers have been thoroughly studied, it is possible to assess the accuracy of the different theoretical approaches in describing the effect that the subtle balance of supramolecular interactions (such as π stacking and hydrogen bonds) has on the excited-state behavior.

The study of π-stacked systems in their excited states is particularly challenging. Indeed, simpler models describing multichromophore spectra on the basis of excitations localized on the chromophore, weakly coupled by exciton coupling, are not fully adequate to describe strongly interacting systems, that is, face-to-face π-stacked systems close to their van der Waals minimum (intermonomer distance $\sim$3–4 Å). In these latter systems, the frontier orbitals can have a substantial overlap and the resulting electronic transitions delocalized over multiple bases. This is indeed the case of the lowest energy bright electronic transitions of stacked adenine nucleobases in polyAde single and double strands [133–136]. In this latter case, our studies in the field provide encouraging indications about the reliability of TD-DFT calculations when based on a suitable functional for the treatment of the excited states in π-stacked nucleobases. Both in stacked adenine dimer and in $Ade_2{\cdot}Thy_2$ stacked tetramer [133–136], PCM/TD-PBE0 calculations (at both the SS-PCM and LR-PCM levels) fully reproduce all the features that experiments show polyAde·polyThy oligomers always exhibit when compared to the spectrum of equimolar mixtures of the corresponding monomers [137, 138]:(i) a weak blue shift of the band maximum, (ii) a strong decrease of the absorption intensity, and (iii) a noticeable shoulder in its redwing. Interestingly different functionals are able to reproduce the above features, but PCM/TD-PBE0 VEE are closer to the experimental band maximum. Those results have been obtained also on a system explictly including the phosphoribose backbone (see Figure 1.4), providing useful indications on the effect of the backbone on the absorption spectrum of DNA.

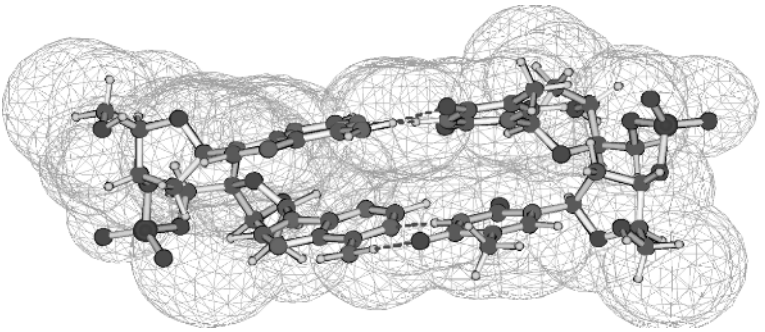

Figure 1.4 Schematic drawing of the $(dT)_2 \cdot (dA)_2$ tetramer, adopting the B-DNA conformation. The PCM cavity used for calculations in solution is also shown.

The transition energy of several dark-excited states falls within the absorption band of the tetramer and the Ade dimer. Some of them have a clear-cut Ade → Ade or Ade → Thy CT character, and their energy is significantly underestimated by PBE0 with respect to CAM-B3LYP or M052X. In order to investigate this point in more detail, we have optimized the (9Methyl-Ade)·(1Methyl-Thy) Watson–Crick hydrogen-bonded pair in the gas phase, computing the lowest energy transitions by using different density functionals [133]. M052X and CAM-B3LYP functionals predict that the A → T CT transition is less stable by ∼0.8 eV than the bright excited state localized on T. This result agrees within 0.15 eV with predictions of ab initio CC2 methods [139, 140].

PBE0 overestimates the stability of intrastrand CT transitions, although the amount of the overestimation is smaller than what was found for Ade → Thy interstrand CT transitions. We recall indeed that the most dramatic failures of "standard" density functionals in treating CT transitions occur in the case of zero overlap between the MOs of the donor and the acceptor molecule [17]. We have computed the absorption spectrum of $(9\text{Methyl-Ade})_2$ in the gas phase by using the B-DNA-like ground-state minimum, optimized in aqueous solution, as reference geometry. CAM-B3LYP and M05-2X predict that the lowest energy 9Methyl-Ade → 9Methyl-Ade CT transition is ∼0.45 eV less stable than the excited states corresponding to the most intense electronic transition. This estimate is in a good agreement with the 0.64 eV value provided by CC2/TZVP calculations on a similar system (two A molecules adopting the experimental B-DNA structure) [139]. As anticipated above, PBE0 instead predicts that the CT transition is ∼0.25 eV more stable than the bright excited state, with a smaller discrepancy with respect to the CC2 results than that found for the interstrand CT transition.

Although the above results confirm that PBE0 suffers from the same deficiencies as standard functionals in properly treating CT transitions, it is expected to deliver a better description of the stacked systems (in both the ground and excited states) than other commmonly used functionals, such as B3LYP, which do not exhibit the correct asymptotic limit. In fact, when applied to the study of cytosine-stacked dimer, TD-PBE0 provides a very accurate description of the dependence of the S_1 energy on the intermonomer distance, in very good agreement with that obtained at the CASPT2 level [141].

As a consequence, a suitable approach for the study of large-size systems could be that of using TD-PBE0 for predicting and interpreting the behavior of the bright excited states or of the "local" dark transitions (e.g., $n \rightarrow \pi^*$ excitations) but correcting the estimate of the CT transitions energy using results from such long-range corrected functionals as CAM-B3LYP and M062X. An alternative could be that of resorting only to these latter functionals, although the description of the bright excited states could be less accurate than that obtained at the TD-PBE0 level.

In any case, it is clear that proper treatment of the solvent effect, both static and dynamical, is fundamental for reliable evaluation of the CT transition's stability in the condensed phase. When using continuum solvation models, a state-specific approach combined with an accurate description of the excited-state electron density (averaging procedures of the excited-state density such as those usually employed in CASPT2 should be avoided) is mandatory, since LR-PCM/TD-DFT strongly underestimates the stability of transition with even partial CT character.

1.7 CONCLUDING REMARKS

In this chapter we have tried to provide a methodological and computational framework for the calculation of the vertical excitation and emission energies of medium/large molecules in solution. Despite its limitations, TD-DFT appears to be a very promising method. It has a very limited computational cost, it is "user friendly," and, when using a suitable functional (PBE0, CAM-B3LYP, M062X, depending on the system/process under investigation), it provides absorption and emission energies within the 0.2–0.3-eV range of the corresponding experimental peaks. Contemporarily, PCM has shown to be a very effective method for including the solvent effect in the calculation of the optical properties. On this ground, we can sketch the basic steps to follow when computing the absorption and emission spectra of a given compound:

1. Ground-state geometry optimization and frequency calculations. DFT/6-31G (d) (in the gas phase) and PCM/DFT/6-31G(d) (in solution) calculations, employing a global hybrid density functional, usually, provide reliable results.

For Absorption Process

2. TD-PBE0/6-31+G(d,p) (in the gas phase) and LR-PCM/TD-PBE0/6-31+G(d,p) (in solution) should provide a good estimate of the VEE, but for Rydberg states where a TZV basis is needed.
3. When looking for a more accurate estimate of the energy difference between the different excited states in solution: (i) SS-PCM/TD-DFT/6-31+G(d,p) calculations and, for hydrogen bonding solvent, (ii) including in the calculation the molecules of the first solvation shell.

For Emission Process

4. Computing the excited-state geometry. TD-PBE0/6-31G(d) (in the gas phase) and LR-PCM/TD-PBE0/6-31G(d) calculations should provide a reliable geometry.

5. TD-PBE0/6-31+G(d,p) (in the gas phase) and LR-PCM/TD-PBE0/6-31+G(d,p) (in solution) should provide a good estimate of the emission energy, although, in solution, a SS-PCM/TD-PBE0/6-31+G(d,p) check is highly recommended.
6. For supramolecular systems TD-PBE0 can understimate the VEE of CT transition. A check using other functionals (as CAM-B3LYP or M06-2X) or computational approaches is highly recommended.
7. When treating hydrogen-bonding solvents, accurate absorption and emission energies can be obtained only when the cybotactic region is explicitly included in the calculations. Mixed continuum–discrete approaches are very effective. Sometimes the choice of the model is not unambiguous but, in any case, for reasonable choices the results are much more accurate than that obtained by using only PCM or purely supramolecular approaches in the gas phase.

In most cases, the above recipes can be directly applied to supramolecular systems containing up to ~150 atoms, providing fairly accurate results. On the other hand, it is important to be aware that any computational approach, when used as a blackbox, can lead to disappointing results, especially when dealing with complex systems/processes. The approaches we have described in this chapter do not yet enable, instead, the calculation of the optical and electronic properties of very large supramolecular systems at the nanoscale. However, the possibility of accurately computing the properties of "meaningful" building blocks (see, e.g., the $Ade_2{\cdot}Thy_2$ tetramer for AT DNA) is an important step toward the definition of effective and reliable multiscale models.

REFERENCES

1. N. Tkachenko, *Optical Spectroscopy Methods and Instrumentations*, Elsevier, Amsterdam, 2006.
2. (a) J. Laane, H. Takahashi, A. D. Bandrauk, Eds., *Structure and Dynamics of Electronic Excited States*, Springer, Berlin, 1998. (b) M. Klessinger, J. Michl, Eds., *Excited States and Photo-Chemistry of Organic Molecules*, VCH, Mannheim, Berlin, 1995.
3. (a) C. H. Wang, *Spectroscopy of Condensed Media*, Academic, New York, 1985. (b) G. R. Fleming, *Chemical Applications of Ultrafast Spectroscopy*, Oxford University, New York, 1986.
4. A. H. Zewail, *Femtochemistry: Ultrafast Dynamics of the Chemical Bond*, World Scientific, Singapore, 1994.
5. M. L. Horbg, J. A. Gardecki, A. Papazyan, M. Maroncelli, *J. Phys. Chem.* **1995**, *99*, 17311.
6. L. P. Lustres, S. A. Kovalenko, M. Mosquera, T. Senyushkina, W. Flasche, N. P. Ernsting, *Angew. Chem. Int. Ed.* **2005**, *44*, 5635.
7. R. M. Christie, *Colour Chemistry*, Royal Society of Chemistry, Cambridge, 1971.
8. M. Grätzel, *Acc. Chem. Res.* **2009**, *42*, 1788–1798.

9. K. Walzer, B. Maennig, M. Pfeiffer, K. Leo, *Chem. Rev.* **2007**, *107*, 1233.
10. S. Verma, G. M. Watt, Z. Mai, T. Hasan, *Photochem. Photobiol.* **2007**, *83*, 996.
11. E. Terreno, D. Delli Castelli, A. Viale, S. Aime, *Chem. Rev.* **2010**, *110*, 3019.
12. M. Olivucci, A. Sinicropi, Computational photochemistry, in *Computational Photochemistry*, Vol. 16, M. Olivucci, Ed., Elsevier, Amsterdam, 2005.
13. W. Domcke, D. R. Yarkony, H. Koppel, Eds., *Conical Intersections: Electronic Structure, Dynamics & Spectroscopy*. (Advanced Series in Physical Chemistry), World Scientific Publishing, Singapore, 2004.
14. B. O. Roos, *Acc. Chem. Res.* **1999**, *32*, 137.
15. B. O. Roos, K. Andersson, M. P. Fülscher, P. A. Malmqvist, L. Serrano-Andres, K. Pierloot, M. Merchán, Multiconflgurational perturbation theory: Applications in electronic spectroscopy, *Adv. Chem. Phys.* **1996**, *93*, 219.
16. L. Gagliardi, B. Roos, *Chem. Soc. Rev.* **2007**, *36*, 893.
17. M. K. Casida, in *Recent Advances in Density Functional Methods*, Part I, D. P. Chong, Ed., World Scientific, Singapore, 1995.
18. K. Burke, J. Werschnik, E. K. U. Gross, *J. Chem. Phys* **2005**, *123*, 62206.
19. R. J. Buenker, S. D. Peyerimhoff, P. J. Bruna, in *Computational Theoretical Organic Chemistry*, I. G. Csizmadia, R. Daudel, Eds., Reidel, Dordrecht, The Netherlands, 1981, p. 91.
20. J. Gauss, in *Encyclopedia of Computational Chemistry*, P. v. R. Schleyer, N. L. Clark, J. Gasteiger, H. F. Schaefer III, P. R. Schreiner, Eds., Wiley, Chichester, 1998, p. 615.
21. R. J. Bartlett, Ed., *Modern Ideas in Coupled-Cluster Methods*, World Scientific, Singapore, 1997.
22. O. Christiansen, H. Koch, P. Jorgensen, *Chem. Phys. Lett.* **1995**, *243*, 409.
23. C. Hättig, F. Weigend, *J. Chem. Phys.* **2000**, *113*, 5154.
24. A. I. Krylov, *Annu. Rev. Phys. Chem.* **2008**, *59*, 433.
25. A. I. Krylov, *Acc. Chem. Res.* **2006**, *39*, 8391.
26. K. Kowalski, P. Piecuch, *J. Chem. Phys.* **2004**, *120*, 1715.
27. S. P. A. Sauer, M. Schreiber, M. R. Silva-Junior, W. Thiel, *J. Chem. Theory Comput.* **2009**, *5*, 555.
28. O. Christiansen, *Theor. Chim. Acta* **2006**, *116*, 106.
29. A. Dreuw, M. Head-Gordon, *Chem. Rev.* **2005**, *105*, 4009.
30. (a) C. J. Cramer, *Essentials of Computational Chemistry*, Wiley, Hoboken, NJ, 2002. (b) F. Jensen, *Introduction to Computational Chemistry*, Wiley, Hoboken, NJ, 2007.
31. A. Dreuw, *Chem. Phys. Chem.* **2006**, *7*, 2259.
32. S. Grimme, *Rev. Comput. Chem.* **2004**, *20*, 153.
33. A. Pezzella, L. Panzella, O. Crescenzi, A. Napolitano, S. Navaratman, R. Edge, E. J. Land, V. Barone, M. d'Ischia, *J. Am. Chem. Soc.* **2006**, *128*, 15490.
34. H. Nakatsuji, K. Hirao, *J. Chem. Phys.* **1978**, *68*, 2053.
35. K. Toyota, I. Mayumi, M. Ehara, M. J. Frisch, H. Nakatsuji, *Chem. Phys. Lett.* **2003**, *367*, 730.
36. A. Köhn, C. Hättig, *J. Chem. Phys.* **2003**, *119*, 5021.
37. P. Celani, H.-J. Werner, *J. Chem. Phys.* **2003**, *119*, 5044.

38. F. Furche, R. Ahlrichs, *J. Chem. Phys.* **2002**, *117*, 7433.
39. (a) C. V. Caillie, R. D. Amos *Chem. Phys. Lett.* **1999**, *308*, *249;* (b) **2000**, *317*, 159.
40. G. Scalmani, M. J. Frisch, B. Mennucci, J. Tomasi, R. Cammi, V. Barone, *J. Chem. Phys.* **2006**, *124*, 094107.
41. B. Mennucci, R. Cammi, Eds., *Continuum Solvation Models in Chemical Physics: From Theory to Applications*, Wiley, New York, 2007.
42. M. Schreiber, M. R. Silva-Junior, S. P. A. Sauer, W. Thiel, *J. Chem. Phys.* **2008**, *128*, 134110.
43. C. M. Marian, N. Gilka, *J. Chem. Theoret. Comp.* **2008**, *4*, 1501.
44. E. K. U. Gross, R. M. Dreizler, *Density Functional Theory*, Springer, Berlin, 1995.
45. V. Barone, R. Improta, N. Rega, *Acc. Chem. Res.* **2008**, *41*, 605.
46. R. Improta, V. Barone, F. Santoro, *Angew. Chem. Int. Ed.* **2007**, *46*, 405.
47. R. Improta, V. Barone, F. Santoro, *J. Phys. Chem. B* **2007**, *111*, 14080.
48. F. Santoro, R. Improta, A. Lami, J. Bloino, V. Barone, *J. Chem. Phys.* **2007**, *126*, 084509.
49. F. Santoro, A. Lami, R. Improta, V. Barone, *J. Chem. Phys.* **2007**, *126*, 184102.
50. F. Santoro, A. Lami, R. Improta, J. Bloino, V. Barone, *J. Chem. Phys.* **2008**, *128*, 224311.
51. Y. Zhao, D. G. Truhlar, *Acc. Chem. Res.* **2008**, *41*, 157.
52. Y. Zhao, D. G. Truhlar, *J. Chem. Theory Comput.* **2005**, *1*, 415.
53. D. Jacquemin, E. A. Perpete, I. Ciofini, C. Adamo, *Acc. Chem. Res.* **2009**, *42*, 326.
54. D. Jacquemin, V. Wathelet, E. A. Perpete, C. Adamo, *J. Chem. Theory Comput.* **2009**, *5*, 2420.
55. D. Jacquemin, E. A. Perpete, I. Ciofini, C. Adamo, *J. Chem. Theory Comput.* **2010**, *6*, 1532.
56. D. Jacquemin, V. Wathelet, E. A. Perpete *J. Phys. Chem. A* **2006**, *110*, 9145.
57. D. Jacquemin, E. A. Perpete, O. A. Vydrov, G. E. Scuseria, C. Adamo, *J. Chem. Phys.* **2007**, *127*, 094102.
58. D. Jacquemin, E. A. Perpete, G. Scalmani, M. J. Frisch, R. Kobayashi, C. Adamo, *J. Chem. Phys.* **2007**, *127*, 094102.
59. M. Dierksen, S. Grimme, *J. Chem. Phys.* **2005**, *122*, 244101.
60. E. Runge, E. K. U. Gross, *Phys. Rev. Lett.* **1984**, *52*, 997.
61. (a) C. Jamorski, M. E. Casida, D. R. Salahub, *J. Chem. Phys.* **1996**, *104*, 5134. (b) M. Petersilka, U. J. Gossmann, E. K. U. Gross, *Phys. Rev. Lett.* **1996**, *76*, 1212. (c) R. Bauernschmitt, R. Ahlrichs, *Chem. Phys. Lett.* **1996**, *256*, 454.
62. R. E. Stratmann, G. E. Scuseria, M. J. Frisch, *J. Chem. Phys.* **1998**, *109*, 8218.
63. M. Wanko, M. Garavelli, F. Bernardi, T. A. Niehaus, T. Frauenheim, M. Elstner, *J. Chem. Phys.* **2004**, *120*, 1674.
64. D. J. Tozer, R. D. Amos, N. C. Handy, B. O. Roos, L. Serrano-Andres, *Mol. Phys.* **1999**, *97*, 859.
65. A. Dreuw, J. L. Weisman, M. Head-Gordon, *J. Chem. Phys.* **2003**, *119*, 2943.
66. A. Dreuw, M. Head-Gordon, *J. Am. Chem. Soc.* **2004**, *126*, 4007.
67. K. Burke, J. Werschnik, E. K. U. Gross, *J. Chem. Phys.* **2005**, *123*, 62206.
68. O. Gritsenko, E. J. Baerends, *J. Chem. Phys.* **2004**, *121*, 655.
69. Y. Tawada, T. Tsuneda, S. Yanagisawa, T. Yanai, K. Hirao, *J. Chem. Phys.* **2004**, *120*, 8425.

70. T. N. Maitra, F. Zhang, R. J. Cave, K. Burke, *J. Chem. Phys.* **2004**, *120*, 5932.
71. N. T. Maitra, *J. Chem. Phys.* **2005**, *122*, 234104.
72. T. Yanai, D. Tew, N. Handy, *Chem. Phys. Lett.* **2004**, *393*, 51.
73. O. A. Vydrov, G. E. Scuseria, *J. Chem. Phys.* **2006**, *125*, 234109.
74. M. A. Rohrdanz, K. M. Martins, J. M. Herbert, *J. Chem. Phys.* **2009**, *130*, 054112.
75. Y. Zhao, D. G. Truhlar, *Theor. Chem. Acc.* **2008**, *120*, 215.
76. Y. Zhao, N. E. Schultz, D. G. Truhlar, *J. Chem. Theoret. Comp.* **2006**, *2*, 364.
77. M. Schreiber, V. Bub, M. P. Fulscher, *Phys. Chem. Chem. Phys.* **2001**, *3*, 3906.
78. J. Tomasi, B. Mennucci, R. Cammi, *Chem. Rev.* **2005**, *105*, 2999.
79. M. Orozco, F. J. Luque, *Chem. Rev.* **2000**, *100*, 4187.
80. (a) J. Gao, *Acc. Chem. Res.* **1996**, *29*, 298. (b) G. Monard, K. M. Merz, Jr., *Acc. Chem. Res.* **1999**, *32*, 904.
81. M. Pavone, O. Crescenzi, G. Morelli, N. Rega, V. Barone, *Theor. Chem. Acc.* **2006**, *116*, 456.
82. S. Miertus, E. Scrocco, J. Tomasi, *J. Chem. Phys.* **1981**, *55*, 117.
83. (a) R. Cammi, S. Comi, B. Mennucci, J. Tomasi, *J. Chem. Phys.* **2005**, *122*, 104513. (b) S. Comi, R. Cammi, B. Mennucci, J. Tomasi, *J. Chem. Phys.* **2005**, *123*, 134512.
84. M. Caricato, B. Mennucci, J. Tomasi, F. Ingrosso, R. Cammi, S. Comi, G. Scalmani, *J. Chem. Phys.* **2006**, *124*, 24520.
85. R. Improta, V. Barone, G. Scalmani, M. Frisch, *J. Chem. Phys.* **2006**, *125*, 54103.
86. R. Improta, G. Scalmani, M. J. Frisch, V. Barone, *J. Chem. Phys.* **2007**, *127*, 74504.
87. M. Cossi, V. Barone, *J. Chem. Phys.* **2001**, *115*, 4708.
88. R. Improta, V. Barone, *J. Mol. Struct. Theochem.* **2009**, *914*, 87.
89. P. Hohenberg, W. Kohn, *Phys. Rev. B* **1964**, *136*, 864.
90. (a) A. D. Becke, *Phys. Rev. A* **1988**, *38*, 3098–100. (b) C. Lee, W. Yang, R. G. Parr, *Phys. Rev. B* **1988**, *37*, 785.
91. J. P. Perdew, K. Burke, M. Ernzerhof, *Phys. Rev. Lett.* **1996**, *77*, 3865.
92. A. D. Boese, N. C. Handy, *J. Chem. Phys.* **2001**, *114*, 5497.
93. A. D. Becke, *J. Chem. Phys.* **1993**, *98*, 5648.
94. C. Adamo, V. Barone, *J. Chem. Phys.* **1999**, *110*, 6158.
95. M. Enzerhof, G. E. Scuseria, *J. Chem. Phys.* **1999**, *110*, 5029.
96. C. Adamo, G. E. Scuseria, V. Barone, *J. Chem. Phys.* **2000**, *111*, 2889.
97. J. Jaramillo, G. E. Scuseria, M. Ernzerhof, *J. Chem. Phys.* **2003**, *118*, 1068.
98. (a) S. K. Ghosh, R. G. Parr, *Phys. Rev. A* **1986**, *34*, 785. (b) J. Tau, J. P. Perdew, V. N. Staroverov, E. Scuseria, *Phys. Rev. Lett.* **2003**, *91*, 146401.
99. M. Levy, J. P. Perdew, *Phys. Rev. B* **1993**, *48*, 11638.
100. E. H. Lieb, S. Oxford, *Int. J. Quantum Chem.* **1981**, *19*, 427.
101. V. Barone, M. Cossi, J. Tomasi, *J. Chem. Phys.* **1997**, *107*, 3210.
102. M. Cossi, V. Barone, *J. Chem. Phys.* **2000**, *112*, 2427.
103. E. J. Baerends, G. Ricciardi, A. Rosa, S. J. A. van Gisbergen, *Coord. Chem. Rev.* **2002**, *230*, 5.
104. M. Pastore, E. Mosconi, F. De Angelis, M. Gratzel, *J. Phys. Chem. C* **2010**, *114*, 7205.

105. (a) F. Neese, *Coord. Chem. Rev.* **2009**, *253*, 526. (b) F. Neese, T. Petrenko, D. Ganyushin, G. Olbrich, *Coord. Chem. Rev.* **2007**, *205*, 288.

106. (a) C. E. Crespo-Hernandez, B. Cohen, P. M. Hare, B. Kohler, *Chem. Rev.* **2004**, *104*, 1977. (b) C. T. Middleton, K. de La Harpe, C. Su, Y. K. Law, C. Crespo-Hernadez, B. Kohler, *Annu. Rev. Phys. Chem.* **2009**, *60*, 13.

107. T. Gustavsson, A. Banyasz, E. Lazzarotto, D. Markovitsi, G. Scalmani, M. J. Frisch, V. Barone, R. Improta, *J. Am. Chem. Soc.* **2006**, *128*, 607.

108. E. Epifanovsky, K. Kowalski, P.-D. Fan, M. Valiev, S. Matsika, A. I. Krylov, *J. Phys. Chem. A* **2008**, *112*, 9983.

109. R. Improta, V. Barone, A. Lami, F. Santoro *J. Phys. Chem. B* **2009**, *113*, 14491.

110. P. M. Hare, C. Crespo-Hernandez, B. Kohler, *Proc. Natl. Acad. Sci. U.S.A.* **2007**, *104*, 435.

111. T. Climent, R. Gonzalez-Luque, M. Merchan, L. Serrano-Andres, *Chem. Phys. Lett.* **2007**, *441*, 327.

112. Y. Mercier, F. Santoro, M. Reguero, R. Improta, *J. Phys. Chem. B* **2008**, *112*, 10769.

113. M. Merchan, R. Gonzalez-Luque, T. Climent, L. Serrano-Andres, E. Rodriguez, M. Reguero, D. J. Pelez, *J. Phys. Chem. B* **2006**, *110*, 26471.

114. L. B. Clark, I. Tinoco, Jr., *J. Am. Chem. Soc.* **1965**, *87*, 11.

115. R. Improta, V. Barone, *J. Am. Chem. Soc.* **2004**, *126*, 14320.

116. F. Santoro, V. Barone, T. Gustavsson, T. Improta, *J. Am. Chem. Soc.* **2006**, *128*, 16312.

117. K. A. Kistler, S. Matsika, *J. Phys. Chem. A* **2009**, *113*, 12396.

118. C. Zazza, A. Amadei, N. Sanna, A. Grandi, G. Chillemi, A. Di Nola, M. D'Abramo, M. Aschi, *Phys. Chem. Chem. Phys.* **2006**, *8*, 1385.

119. V. Ludwig, K. Coutinho, S. Canuto, *Phys. Chem. Chem. Phys.* **2007**, *9*, 4907.

120. J. M. Olsen, K. Aidas, K. V. Mikkelsen, J. Kongsted, *J. Chem. Theoret. Comp.* **2010**, *6*, 249.

121. R. Improta, V. Barone, *Chem. Rev.* **2004**, *104*, 1231.

122. M. Chahinian, H. B. Seba, B. Ancian, *Chem. Phys. Lett.* **1998**, *285*, 337.

123. M. P. Gaigeot, M. Sprik, *J. Phys. Chem. B* **2004**, *108*, 7458.

124. V. Karunakaran, K. Kleinermanns, R. Improta, S. A. Kovalenko, *J. Am. Chem. Soc.* **2009**, *131*, 5839.

125. M. Maroncelli, G. R. Fleming, *J. Chem. Phys.* **1987**, *86*, 6221.

126. (a) Y. Kimura, *J. Chem. Phys.* **1999**, *111*, 5474. (b) T. Gustavsson, L. Cassara, V. Gulbinas, G. Gurzadyan, J. C. Mialocq, S. Pommeret, M. Sorgius, P. van der Meulen, *J. Phys. Chem. A* **1998**, *102*, 4229. (c) F. Ingrosso, B. M. Ladanyi, B. Mennucci, G. Scalmani, *J. Phys. Chem B* **2006**, *110*, 4953.

127. B. A. Pryor, P. M. Palmer, Y. Chen, M. R. Topp, *Chem. Phys. Lett.* **1999**, *299*, 536.

128. A. Muhlpfordt, R. Schanz, N. P. Ernsting, V. Farzdtinov, S. Grimme, *Phys. Chem. Chem. Phys.* **1999**, *1*, 3209.

129. A. Chowdhury, S. A. Locknar, L. L. Premvardham, L. A. Peteanu, *J. Phys. Chem. A* **1999**, *103*, 9614.

130. R. Kanya, Y. Ohshima, *Chem. Phys. Lett* **2003**, *370*, 211.

131. S. Carlotto, A. Polimeno, C. Ferrante, C. Benzi, V. Barone, *J. Phys. Chem. B* **2008**, *112*, 8106.

132. L. M. Frutos, T. Andruniow, F. Santoro, N. Ferré, M. Olivucci, *Proc. Nalt. Acad. Sci. U.S.A.* **2007**, *104*, 7764.
133. F. Santoro, V. Barone, R. Improta, *J. Am. Chem. Soc.* **2009**, *131*, 15232.
134. R. Improta, *Phys. Chem. Chem. Phys.* **2008**, *10*, 2656.
135. F. Santoro, V. Barone, R. Improta, *Chem. Phys. Chem.* **2008**, *9*, 2531.
136. F. Santoro, V. Barone, R. Improta, *Proc. Natl. Acad. Sci. U.S.A.* **2007**, *104*, 9931.
137. D. Markovitsi, T. Gustavsson, F. Talbot, *Photochem. Photobiol. Sci.* **2007**, *6*, 717.
138. D. Onidas, T. Gustavsson, E. Lazzarotto, D. Markovitsi, *J. Phys. Chem. B* **2007**, *111*, 9644.
139. A. W. Lange, J. M. Herbert, *J. Am. Chem. Soc.* **2009**, *131*, 3913.
140. S. Perun, A. L. Sobolewski, W. Domcke, *J. Phys. Chem. A.* **2006**, *110*, 9031.
141. F. Santoro, V. Barone, R. Improta, *J. Comp. Chem.* **2008**, *29*, 957.